Title

Understanding the role of the ground surface in HONO vertical structure: High resolution vertical profiles during NACHTT-11

Permalink

https://escholarship.org/uc/item/49r6w7zj

Journal

Journal of Geophysical Research: Atmospheres, 118(17)

ISSN

2169-897X

Authors

VandenBoer, Trevor C
Brown, Steven S
Murphy, Jennifer G
et al.

Publication Date

2013-09-16

DOI

10.1002/jgrd.50721

Copyright Information

Peer reviewed

Understanding the role of the ground surface in HONO vertical structure: High resolution vertical profiles during NACHTT-11

Trevor C. VandenBoer,[1,2] Steven S. Brown,[3] Jennifer G. Murphy,[1] William C. Keene,[4] Cora J. Young,[2,3,5] A. A. P. Pszenny,[6] S. Kim,[7,8] Carsten Warneke,[3,5] Joost A. de Gouw,[3,5] John R. Maben,[4] Nicholas L. Wagner,[3,5] Theran P. Riedel,[9] Joel A. Thornton,[9] Daniel E. Wolfe,[3,5] William P. Dubé,[3,5] Fatma Öztürk,[10] Charles A. Brock,[3] Nicole Grossberg,[11] Barry Lefer,[11] Brian Lerner,[3] Ann M. Middlebrook,[3] and James M. Roberts[3]
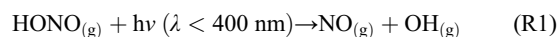
[1] A negative-ion proton-transfer chemical ionization mass spectrometer was deployed on a mobile tower-mounted platform during Nitrogen, Aerosol Composition, and Halogens on a Tall Tower (NACHTT) to measure nitrous acid (HONO) in the winter of 2011. High resolution vertical profiles revealed (i) HONO gradients in nocturnal boundary layers, (ii) ground surface dominates HONO production by heterogeneous uptake of NO_2, (iii) significant quantities of HONO may be deposited to the ground surface at night, (iv) daytime gradients indicative of ground HONO production or emission, and (v) an estimated surface HONO reservoir comparable or larger than integrated daytime HONO surface production. Nocturnal integrated column observations of HONO and NO_2 allowed direct evaluation of nocturnal ground surface uptake coefficients for these species ($\gamma_{NO2, surf}=2 \times 10^{-6}$ to 1.6×10^{-5} and $\gamma_{HONO, surf}=2 \times 10^{-5}$ to 2×10^{-4}). A chemical model showed that the unknown source of HONO was highest in the morning, 4×10^6 molecules $cm^{-3} s^{-1}$ (600 pptv h^{-1}), declined throughout the day, and minimized near 1×10^6 molecules $cm^{-3} s^{-1}$ (165 pptv h^{-1}). The quantity of surface-deposited HONO was also modeled, showing that HONO deposited to the surface at night was at least 25%, and likely in excess of 100%, of the calculated unknown daytime HONO source. These results suggest that if nocturnally deposited HONO forms a conservative surface reservoir, which can be released the following day, a significant fraction of the daytime HONO source can be explained for the NACHTT observations.

1. Introduction

[2] Nocturnal production of nitrous acid (HONO) has been often considered as a reservoir for OH radicals that may be released by photolysis in the early morning hours (R1). While production is thought to be dominated by a heterogeneous process (R2), attribution of aerosol versus ground surfaces, and the associated implications for radical chemistry, has been limited to a few studies of vertical gradients [*Kleffmann et al.*, 2003; *Sörgel et al.*, 2011a; *Villena et al.*, 2011; *Wong et al.*, 2011; *Young et al.*, 2012; *Yu et al.*, 2009; *Zhang et al.*, 2009].

$$HONO_{(g)} + h\nu \ (\lambda < 400 \ nm) \rightarrow NO_{(g)} + OH_{(g)} \qquad (R1)$$

$$2 \ NO_{2(g)} + H_2O_{(ads)} \rightarrow HONO_{(g)} + HNO_{3(ads)} \qquad (R2)$$

$$NO_{(g)} + OH_{(g)} + M \rightarrow HONO_{(g)} + M \qquad (R3)$$

[3] Although the heterogeneous HONO production reaction (R2) is second-order in NO_2, the mechanism for the conversion of NO_2 at surfaces remains unclear [*Finlayson-Pitts*, 2009]. The nighttime production of HONO from NO_2 was first inferred from measured HONO mixing ratios in polluted regions in excess of 5 parts per billion (ppbv) [*Perner and Platt*, 1979; *Platt et al.*, 1980]. Nighttime mixing ratios of HONO this high can still be observed in some locations [*Li et al.*, 2010, 2011; *Villena et al.*, 2011], but are typically on the order of 1–2 ppbv. Following sunrise, HONO produced at night was assumed to have photolyzed completely (e.g., 5–10 min lifetime) when mixing ratios fell below instrumental detection limits, near 200 parts per trillion (pptv). Recent measurements of HONO with high sensitivity (10 min or faster observation intervals, detection limits < 10 pptv) reveal real daytime HONO mixing ratios of several tens to 100 pptv [*Heland et al.*, 2001; *Kleffmann and Wiesen*, 2008; *Kleffmann et al.*, 2006; *Roberts et al.*, 2010; *Stutz et al.*, 2002, 2010; *Wong et al.*, 2012; *Zhang et al.*, 2009]. These state-of-the-science instruments also confirmed the presence of highly variable photostationary HONO mixing ratios (i.e., the daytime minimum mixing ratio of HONO maintained against photolysis) ranging from 10 to 1000 pptv during midday [*Acker et al.*, 2006; *Elshorbany et al.*, 2009, 2012; *Kleffmann et al.*, 2005; *Sörgel et al.*, 2011b; *Su et al.*, 2008a; *Wong et al.*, 2012; *Zhou et al.*, 2011]. The production rate of HONO (P_{HONO}) required to sustain these daytime mixing ratios ranges from a few hundred pptv per hour to over 1 ppbv per hour, far exceeding the known gas phase source by reaction of OH and NO (R3, e.g., with 1 ppbv NO, 5×10^6 molecules cm^{-3} OH, $P_{HONO} = 140$ pptv h^{-1}) and the heterogeneous surface reaction of NO_2 on the sum of ground and particle surfaces (R2). This excess daytime HONO indicates that an additional source or multiple sources of HONO exist during daylight hours, which might contribute 30% to 50% of OH production throughout the day in the summer [*Alicke et al.*, 2003; *Elshorbany et al.*, 2012; *Kleffmann et al.*, 2005; *Volkamer et al.*, 2010; *Young et al.*, 2012]. The daytime production of HONO and its influence on chemistry is less well studied in winter atmospheres when, relative to summer, substantially less OH is produced from O(^{1}D) and other photochemical pathways (S. Kim et al., The primary and recycling sources of OH during the NACHTT-2011 campaign, submitted to *Journal of Geophysical Research: Atmospheres*, 2013).

[4] Laboratory studies have elucidated several alternative reaction pathways for the formation of daytime HONO involving NO_2 and photoexcited surface substrates (e.g., R4), such as soot [*Ammann et al.*, 1998; *Aubin and Abbatt*, 2007; *Gerecke et al.*, 1998; *Khalizov et al.*, 2010; *Monge et al.*, 2010], TiO_2 [*Bedjanian and El Zein*, 2012; *Langridge et al.*, 2009; *Ndour et al.*, 2009; *Ndour et al.*, 2008], humic acid [*Bartels-Rausch et al.*, 2010; *Stemmler et al.*, 2006, 2007], and solid organic films [*Brigante et al.*, 2008; *George et al.*, 2005; *Gutzwiller et al.*, 2002]. However, extrapolation of lab results to real surfaces remains challenging. Their contributions to the required production rate are either much smaller than the source inferred from field observations, or they have proven difficult to quantify [*Sörgel et al.*, 2011b]. Loss of HONO by reaction with OH (R5) and photolysis of orthonitrophenols are possible minor contributors to the

daytime HONO budget [*Bejan et al.*, 2006], with the latter not yet evaluated via direct measurement.

$$NO_{2(g)} + [R - H]^* \rightarrow HONO_{(g)} + [R'] \qquad (R4)$$

$$HONO_{(g)} + OH_{(g)} \rightarrow NO_{2(g)} + H_2O_{(g)} \qquad (R5)$$
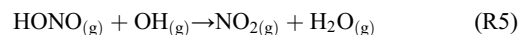
[5] Similarly, photolysis of surface adsorbed nitric acid has been suggested as a HONO source, but yields of HONO from this process remain poorly understood [*Li et al.*, 2012; *Zhou et al.*, 2011; *Ziemba et al.*, 2010]. Reaction of electronically excited NO_2 with water vapor [*Li et al.*, 2008] was also proposed as a major formation pathway for daytime HONO but has since been shown to be a two photon process [*Amedro et al.*, 2011] of little relevance under atmospheric conditions [*Czader et al.*, 2012; *Ensberg et al.*, 2010; *Sörgel et al.*, 2011b; *Wong et al.*, 2012]. Therefore, the source(s) that generate most of the observed HONO during daytime are unknown. Whether this production occurs predominantly in the gas phase, on aerosol surfaces, or on the ground surface remains an open question.

[6] A few studies have evaluated the relative importance of aerosol and ground surfaces in the production of nighttime HONO via (R2). Reactions at the ground surface have been suggested as the most important HONO source based on measured vertical gradients and fluxes of HONO [*Harrison and Kitto*, 1994; *Harrison et al.*, 1996; *Kleffmann et al.*, 2003; *Lammel and Perner*, 1988; *Lammel and Cape*, 1996; *Stutz et al.*, 2002; *Su et al.*, 2008b; *Villena et al.*, 2011; *Wong et al.*, 2011; *Zhang et al.*, 2009]. Other investigations have interpreted surface level measurements in the absence of vertical information to suggest that aerosols enhance HONO production [*Bröske et al.*, 2003; *Reisinger*, 2000; *Su et al.*, 2008b].

[7] Few observations of near real-time HONO vertical gradients have been made [*Kleffmann et al.*, 2003; *Wong et al.*, 2012; *Zhang et al.*, 2009]. Those that have been made are limited by measurement frequency and vertical resolution between the surface, nocturnal boundary layer, and residual layer of the previous day's convective boundary layer. These limitations have been due to the following: (i) the capacity of the available infrastructure to conduct vertical profiling and (ii) the ability of instrumentation to quickly and accurately measure HONO mixing ratios along with other key analytes (e.g., NO_2, NO, and aerosol surface area). An interesting feature of previous vertical gradient and in situ observations is that nighttime temporal profiles of HONO mixing ratios often exhibited a relatively rapid rise after sunset followed by a plateau toward the end of the night which would be consistent with an approach to steady state between production and an undetermined loss process, as proposed by *Stutz et al.* [2002]. This loss has been represented by dry deposition in models [*Sörgel et al.*, 2011b; *Wong et al.*, 2011] and directly observed over the open ocean [*Wojtal et al.*, 2011], but the loss mechanism and fate of HONO in the terrestrial nocturnal atmosphere requires further exploration. The rate of HONO dry deposition is a function of nocturnal boundary layer height and stability [*Geyer and Stutz*, 2004; *Wong and Stutz*, 2010; *Wong et al.*, 2011]. Only recently has this loss process been considered as potentially reversible from observations made over water bodies in

a polluted marine boundary layer [*Wojtal et al.*, 2011] or if significant amounts of water (e.g., in soil pores [*Su et al.*, 2011]) are available as a reservoir at the surface.

[8] Here we report the first continuous vertical profiles measurements of HONO and related species at both high time resolution (< 10 min per profile) and vertical resolution (< 10 m over 250 m elevation). Results are interpreted in conjunction with chemical model calculations to evaluate (i) the heterogeneous formation and loss of HONO on the ground at night, (ii) the production of HONO during daytime, and (iii) the potential for HONO lost to the ground at night to be a significant fraction of the unknown daytime source.

2. Methods

2.1. Site Description and Instrumentation

[9] A comprehensive site description for NACHTT and atmospheric measurement history for this region can be found in the campaign overview by *Brown et al.* [2013]. Briefly, the NACHTT field campaign was located in Colorado at the Boulder Atmospheric Observatory (BAO) (40°03′00″N, 105°00′14″W) [*Kaimal and Gaynor*, 1983] from 17 February to 14 March 2011. The main sampling platform was a 300 m triangular open-frame tower, outfitted with an externally mounted instrument carriage (the Portable Instrument Shelter with Amenities, PISA). The elevator was electrically powered (no emissions at the point of sampling). The PISA reached a maximum height of 270 m above ground level (AGL) during NACHTT. Single vertical transects took less than 10 min (< 20 min per round trip). During high wind events (> 12 m s^{-1}), the carriage was kept stationary at or below 40 m AGL for safety. The PISA housed a suite of instruments including: a meteorology station, GPS and analog height instrumentation, an ultra-high sensitivity aerosol spectrometer for number size distributions of sub-μm diameter aerosols, an aerosol mass spectrometer for nonrefractory composition of sub-μm diameter aerosols, two chemical ionization mass spectrometers (CIMS) for quantitative measurements of $ClNO_2/N_2O_5/Cl_2$ using I$^-$ reagent ion [*Riedel et al.*, 2012] and for $HCl/HONO/HNCO/HCOOH/HNO_3$ using CH_3COO^- reagent ion [*Roberts et al.*, 2010; *Veres et al.*, 2008, 2011], and a cavity ring-down spectrometer for $NO/NO_2/O_3/NO_3/N_2O_5$ [*Wagner et al.*, 2011]. Measurements were made between 0.1 and 1 Hz by each instrument.

[10] An externally mounted sampling platform was installed on the tower at a fixed height of 22 m AGL. HONO, HNO_3, HCl, HCOOH, CH_3COOH, and NH_3 were sampled over 2 h intervals from the platform with tandem mist chambers and analyzed on site by high performance ion chromatography (MC-IC) usually within 1 h after recovery [*Keene et al.*, 2006; *Young et al.*, 2013]. A separate set of ground instruments was located approximately 20 m south of the main tower. These included measurements of photolysis rate constants using a filter radiometer mounted at 10 m AGL and in situ OH by another CIMS [*Eisele and Tanner*, 1991; *Petäjä et al.*, 2009; *Tanner et al.*, 1997] at 2 m AGL.

2.2. Negative-Ion Proton-Transfer Mass Spectrometer (NI-PT-CIMS)

[11] The NI-PT-CIMS has been described previously by *Veres et al.* [2008] and *Roberts et al.* [2010], and its application to these measurements is described below. During the

NACHTT field campaign, the NI-PT-CIMS quantitatively measured the gas phase acids HCl, HONO, HNCO, HCOOH, and HNO_3 at m/z 35, 42, 45, 46, and 62, respectively, in addition to qualitative measurement of acrylic acid ($C_3H_4O_2$), propionic acid ($C_3H_5O_2$), and HBr at m/z 71, 73, and 80. Ion signals were collected using 1 s dwell periods on each ion, and the CH_3COO^- reagent ion (m/z 59), resulting in a 0.1 Hz measurement rate. Dry nitrogen gas for the ion source was supplied to the instrument via a Pressurized Liquid Nitrogen system on board the carriage. A custom sampling inlet (Figure S1 in the supporting information) was devised for the NI-PT-CIMS to perform online background measurements and calibration checks, which are described in detail in the supporting information.

[12] Offline calibrations performed on the NI-PT-CIMS were collected at 1 Hz, with one or more supporting measurements of the HONO calibration gas made by chemiluminescence or ion chromatography, similar to those described by *Roberts et al.* [2010] and *Veres et al.* [2008] (details in the supporting information). Calibrations of HONO during NACHTT ($n = 4$) showed responses of 10.4 ± 1.8 counts pptv^{-1}, similar to that previously reported [*Roberts et al.*, 2010], with high linearity ($R^2 \geq 0.999$) between 500 and 5000 pptv. The instrument detection limit, determined as 2σ of ion counts in a 10 min background, was 3.8 pptv at 10 s time resolution (i.e., 0.1 Hz). The NI-PT-CIMS HONO accuracy, determined by variability in calibration slopes before, during, and after the campaign, was 17%. Calibrations bracketing a given measurement period, as an average, were used to account for variability in the instrument response. Calibrations of the standard gases HCl and HNO_3 had accuracies of 10% and 14%, respectively, showing complementary results for the stability of the NI-PT-CIMS sensitivity throughout the campaign. Mixing ratios of HONO measured by the NI-PT-CIMS within ± 10 m of the sampling inlet for the MC-IC were averaged over the MC-IC sampling intervals and intercompared. An orthogonal least distance fit of the paired CIMS versus MC-IC data ($n = 117$) yielded a slope of 1.38 ± 0.05, an intercept of 3 ± 12, and $R^2 = 0.87$. Different sampling rates for the two techniques and discontinuities in sampling times for paired data, resulting from the vertical motion of the NI-PT-CIMS past the fixed MC-IC inlet, contributed to variability in the two data sets. However, the slope of the regression indicated that the NI-PT-CIMS measured consistently higher (averaging 38%) mixing ratios of HONO, particularly above 200 pptv (section B, Figure S2). The slope for a regression of the subset of paired data for mixing ratios less than 200 pptv ($n = 64$) diverged from a 1:1 line by 13%. Causes for this systematic divergence are not known, but these results suggest that HONO measured via NI-PT-CIMS may be biased high or HONO measured by MC-IC may be biased low by up to 38% at the upper end of the mixing ratio range observed and by about 13% at the lower end.

[13] Temperature-dependent inlet transmission of HONO was characterized using a method similar to *Veres et al.* [2008] and *Roberts et al.* [2010]. Moderate mixing ratios, on the order of 1 ppb, were modulated with dry nitrogen gas as a blank to characterize the response time in reaching maximum signal or minimum background ion counts. Temperatures between 30°C and 60°C were tested to optimize the response time to be 0.6 s, or less, to reach 95% of
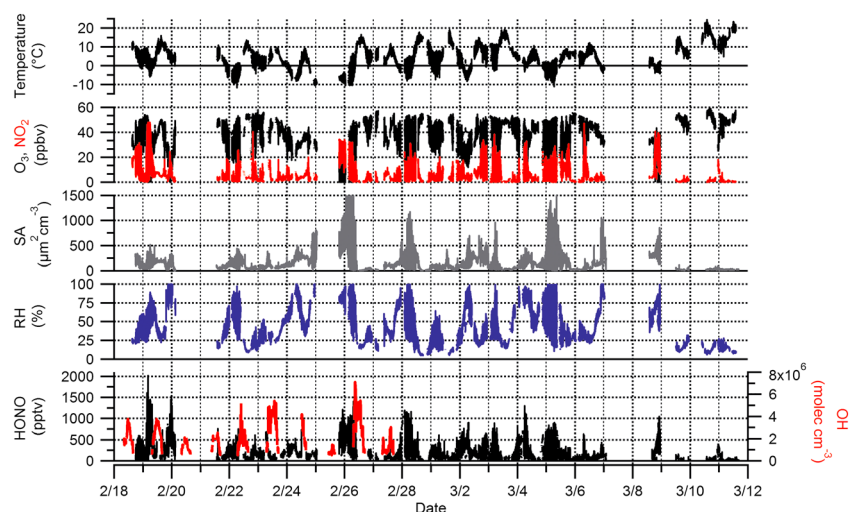
Figure 1. Continuous field observations used in the analysis of HONO nighttime formation during NACHTT-11, filtered to remove wind speeds greater than $6\,\mathrm{m\,s}^{-1}$ and periods of stationary height measurements, in order to select for data collected when the tower was most impacted by local emissions from the surrounding urban area and to avoid bias from prolonged sampling under stationary conditions, respectively. Daytime OH measurements were made only for the first 10 days of the campaign. Fine structure superimposed on the time series is the result of vertical variations as the instrument carriage transits the tower, as described further below.

full signal between blank and stable calibration mixing ratios and vice versa. The transmission of HONO through the inlet was faster than 0.6 s at all temperatures. The transmission times for all acids in the short heated inlet design used during NACHTT were at least a factor of 4 better than those previously reported for this instrument [*Roberts et al.*, 2010], when the inlet was heated to 60°C, providing adequate spatial resolution for the rapid vertical profile measurements made during this campaign. Finally, breakthrough investigations showed 0.5% transmission of the HONO calibration gas through the blank channel across the range of 500–7000 pptv. These values held, even after operating in the field for several weeks. The data set was corrected for this accordingly. Interferences in this HONO measurement from NO_2 and other compounds were also accounted for (section A in the supporting information).

3. Results and Discussion

3.1. Nocturnal Nitrous Acid (HONO)

3.1.1. General Observations and Vertical Profile Analysis

[14] Figure 1 depicts the measurements used to evaluate HONO formation and processing. Four different meteorological regimes were characterized during the campaign. From 18 to 25 February, the region was impacted by cold, moist conditions; temperatures varied over diel cycles between −10°C and 10°C, and relative humidities between 30% and 90%. This was followed by a warmer moist period from 26 February to 3 March, during which maximum temperatures approached 20°C and rarely fell below 0°C at night. Conditions similar to those of the first period occurred from 4 to 9 March, with a freezing fog event on the night of 4–5 March before starting to warm again at the end of the campaign. Further details on site characteristics can be found in *Brown et al.* [2013]. The concentration of O_3 during periods of minimum local urban influence at this site is on the order of 50 ppb (Figure 1). This background mixing ratio of O_3 (which was higher than that associated with polluted air masses from the Denver urban area) was used along with potential temperature to identify stable nocturnal boundary layers (NBLs) throughout the campaign. Details on the process for identifying NBLs are available in section C of the supporting information (Figure S3).

[15] At night, the highest HONO mixing ratios were measured near the surface, building up to greater than 1 ppb on five nights (19, 20, and 28 February and 4 and 8 March), and approximately 500 pptv on the rest of the nights (Figure 1). Vertical stratification of HONO varied between nights. On some nights, the NBL formed from a stable surface layer. On other nights, the NBL height was stable and a pre-existing surface layer was not identifiable within 2 h of sunset. This NBL variability can be observed in Figure 2a by the change in height of HONO vertical gradients on a night-to-night basis. The presence of a stable boundary layer has been suggested as a key condition for the accumulation and stratification of HONO at night in models [*Geyer and Stutz*, 2004; *Vogel et al.*, 2003; *Wong et al.*, 2011] and in field observations of HONO vertical profiles [*Kleffmann et al.*, 2003; *Wong et al.*, 2011; *Zhang et al.*, 2009]. Higher HONO mixing ratios in surface layers are consistent with the hypothesis that reactions on ground surfaces dominate the heterogeneous production of HONO from NO_2 during the campaign.

[16] Nights when stable layers of air were formed at the surface generally had low wind speeds ($<6\,\mathrm{m\,s}^{-1}$) and showed higher HONO mixing ratios in air arriving from all directions, suggesting a local source (Figure 3). Vertical profile data were used when wind speeds were less than $6\,\mathrm{m\,s}^{-1}$ and from periods of near-continuous collection of vertical measurements to avoid bias in observations from prolonged stationary sampling conditions and to select for
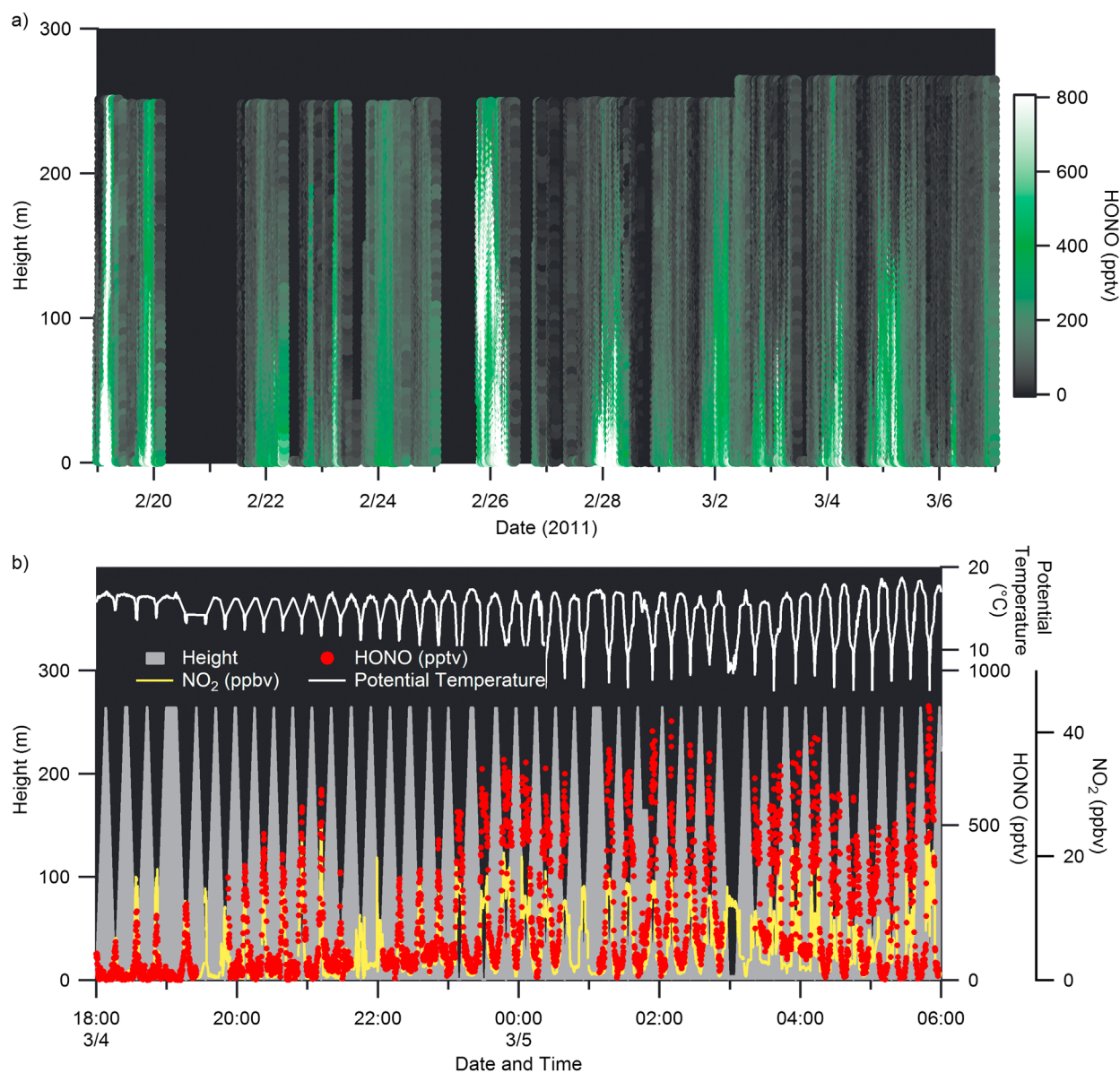
Figure 2. (a) Curtain plot of HONO vertical mixing ratios measured by the NI-PT-CIMS during NACHTT-11. Note that the color scale ends at 800 pptv of HONO to optimize contrast in the vertical gradients of HONO observed even though mixing ratios up to 2 ppbv were observed during the campaign. Mixing ratios of HONO in excess of 800 pptv are displayed as white data points. (b) Vertical profiles of HONO (red circles, 0–1000 pptv), NO$_2$ (yellow line, 0–50 ppbv), and potential temperature (5–20) in real time as a function of height on 4 March 2011.

data collected when the tower was impacted by local chemistry. High wind events occurred on 19, 23, 26, and 28 February and 3 March, inhibiting the accumulation of HONO. The presence of nocturnal thermal inversions at the surface was determined according to the method of *Brown et al.* [2007] using potential temperature and ozone measurements (Figure 2b). Under such conditions, the integrated column rate of change in HONO (i.e.,

$$\text{dHONO}_{\text{column}} \, / \text{d}t = \left(\int_{h=0m}^{250m} [\text{HONO}] \text{d}h \right) / \text{d}t \,,\text{ see section}$$

3.1.4) and NO$_2$ was used to constrain both surface production and loss of HONO. Nine occasions (18–19, 19–20, 21–22, and 27–28 February, 28 February to 1 March, 1–2, 2–3, 4–5, and 7–8 March) had NBLs confined below the

top of the PISA transit height, which are presented in section D of the supporting information (Figure S4).

3.1.2. HONO Production and Loss in the NBL: Observations, Modeling, and Utility of HONO/NO$_2$

[17] Vertical profile data were binned in bihourly intervals and 10 m vertical bins from the surface to 250 m AGL to evaluate underlying chemical processes in HONO production and loss. In general, the depth of the gradient in HONO was found to increase with the depth of the observed nocturnal boundary layer, higher mixing ratios of NO$_2$, and time. Some of the observed changes within a given night, however, are due to transport and emissions of NO$_2$ in different air masses and not strictly chemical processing. For illustrative purposes and to support arguments made below, a simple box model
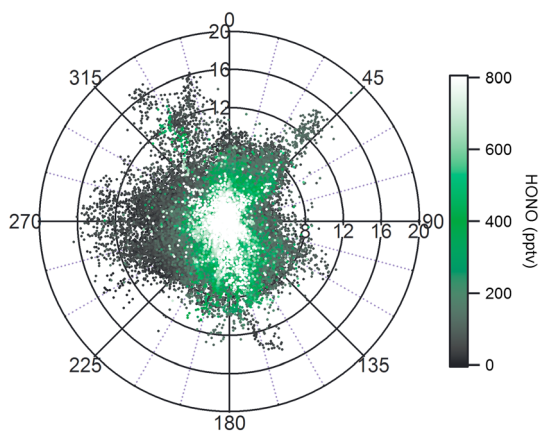
Figure 3. Windrose plot of HONO observations with 0° as north. Rings around the origin denote increasing wind speeds in 4 m s^{-1} intervals up to 20 m s^{-1}. HONO mixing ratios have been sorted from highest to lowest to depict the local nature of HONO formation at night. The Colorado Front Range is located roughly 25 km to the west.

representation of only the chemical processes involved in HONO production at night, compared to observations at the surface on 27–28 February, can be found in section E of the supporting information (Figures S5 and S6). Similar profiles were observed on nine other nights during the campaign, although there is considerable variation in the vertical structure due to: (i) the presence and depth of surface and NBLs, (ii) the amount of NO_2, and (iii) the relative humidity at the surface (Figure S7). The linear least squares regression correlations of HONO to NO_2 within the NBL on these nights are generally high ($R^2 \geq 0.8$), particularly from 22 to 06 h (Figure S7, Table S1). Figure 4 depicts the night of 27–28 February as an example of the evolution of the HONO vertical profile with increasing NBL height and is discussed in detail below.

[18] Mixing ratios of HONO increased at the surface by a small amount in the first 2 h of the night, followed by an increase of 100, 500, 750, and 850 pptv in each subsequent 2 h interval (Figure 4). During this same period, the mixing ratio of NO_2 at the surface increased from 7 to 16 ppbv, with transport of an 18 ppbv plume at the surface between 00 and 02 h (Figure S5). The stable NBL confined emissions of NO_2 at the surface, enhancing HONO formation. The HONO to NO_2 ratios (HONO/NO_2) show nearly flat profiles throughout the column, increasing from $3.5\% \pm 0.4\%$ between 18 and 20 h to $7.6\% \pm 0.6\%$ between 04 and 06 h. Relative humidity remained near 80% at the surface and 35% above the NBL throughout the night. Hydrated aerosol surface area (data not shown) in the residual layer, averaged over the total depth, was less than 160 µm^2 cm^{-3} throughout the night (range: 62–158 µm^2 cm^{-3}). Below 30 m AGL, the hydrated aerosol surface area was 300 µm^2 cm^{-3} from 10 to 04 h and reached a maximum 2 h average of 742 µm^2 cm^{-3} between 04 and 06 h. The accumulation of HONO near the surface stabilized near 1000 pptv from 02 to 06 h, while the HONO/NO_2 ratio continued to increase from $6.8\% \pm 0.4\%$ between 02 and 04 h to $7.6\% \pm 0.6\%$ between 04 and 06 h. There was considerable variability in HONO and HONO/NO_2 within and between nights throughout NACHTT-11, presumably due to changes in NO_2 emission sources and transport effects (Figure S4). However, absolute HONO mixing ratios and HONO/NO_2 consistently approached a steady state plateau on nights with NBLs. Two possible chemical processes could account for the buildup and near steady state observed in the HONO mixing ratio and HONO/NO_2 (Figures S5 and S6): (i) loss of HONO to surfaces by dry deposition, and/or (ii) a slower rate of NO_2 heterogeneous conversion to HONO via (R2) than has been reported. The plausibility and implications of each explanation was explored by comparing observations against the chemical model mentioned above. These
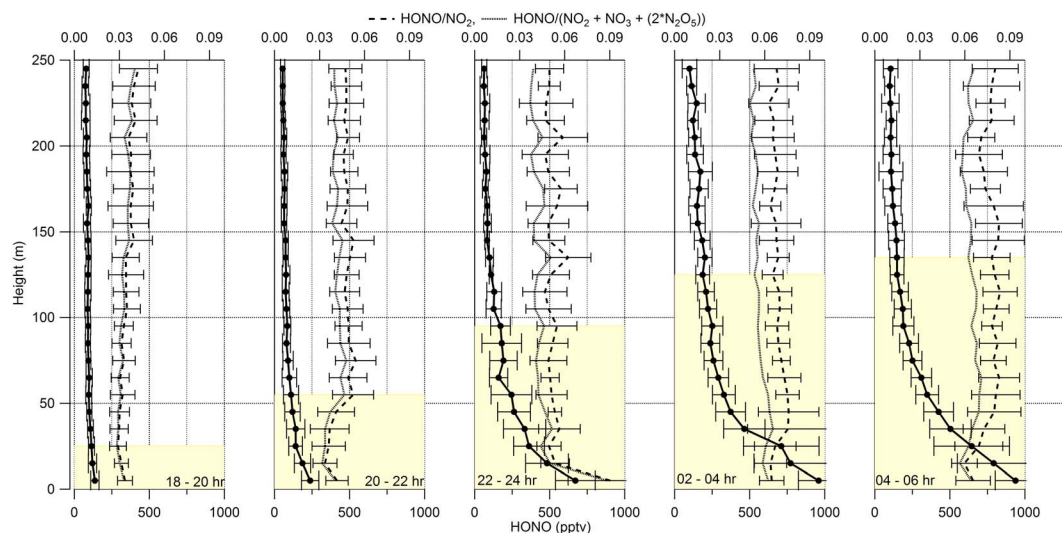

Figure 4. Evolution of HONO (solid line ± 1σ) vertical profiles from 18:00 to 06:00 MST in 2 h bins (excluding 00–02 h due to instrument maintenance) on 27–28 February. Each time bin shows the average vertical structure of HONO in pptv on the bottom axis. The height of the thermal inversion layer (i.e., NBL) was not constant throughout the night and is denoted in each bin by the shaded yellow bar. Vertical profiles of the ratios HONO/NO_2 (dashed line ± 1σ) and HONO/(NO_2 + NO_3 + (2*(N_2O_5))) (dotted line) on the top axis, show vertical structure in the nocturnal boundary layer.

are discussed below using the 27–28 February observations shown in Figure 4.

[19] We suggest that the ground surface dominates both processes because heterogeneous HONO production from NO_2 and, consequently, HONO/NO_2 are limited by transport of the molecules to a surface (i.e., a resistance) and their reaction probabilities. In these surface interactions, the ground has a much greater surface area than the aerosol, even when assuming the ground is a planar surface (e.g., in a 150 m deep NBL, the ground surface area is 6700 $\mu m^2 cm^{-3}$, versus the 27–28 February average of 146 $\mu m^2 cm^{-3}$ hydrated submicron aerosol surface area, or even the maximum of 742 $\mu m^2 cm^{-3}$ at the surface). The transport resistance term is negated in HONO production because of the small uptake coefficient of NO_2 on surfaces, between 1×10^{-6} and 1×10^{-5}, effectively allowing the summed surface area and consequently the ground to dominate the chemistry (see section 3.1.4). In contrast, if the NO_2 uptake were more efficient (e.g., $\gamma > 10^{-4}$ for N_2O_5) (N. L. Wagner et al., N_2O_5 uptake coefficients determined from ambient wintertime measurements, submitted to *Journal of Geophysical Research: Atmospheres*, 2013), aerosol surfaces would be expected to become more influential on the lifetime of the reactive gas. Thus, the production of HONO from reaction of NO_2 on the ground surface leads to the buildup of HONO near the ground.

[20] During NACHTT-11, HONO/NO_2 observed within 10 m of the surface increased with time during the night, which is consistent with HONO production occurring there. When mixing ratios of HONO at the surface stabilize during the last 4 h of the night, the HONO/NO_2 ratio was also observed to approach steady state (Figure 4). The increases in both HONO and HONO/NO_2 with time become smaller as the night progresses. These increases are, in part, due to vertical transport, but this only appears to be happening quickly within 50 m of the surface. To approximate these values in our model, either the production of HONO from NO_2 at the surface is slower than expected from values determined in previous work by up to a factor of 5, or there is an additional HONO loss process at the surface (Figures S5 and S6). Since the values for reactive uptake of NO_2 at the surface are reasonably well established, the HONO and HONO/NO_2 observations in Figure 4 are most consistent with loss of HONO to the surface. During NACHTT-11, this sink was rapid enough for HONO to approach steady state in 12 to 13 h, meaning that the rate coefficient is about 4 to 5 times faster than this interval, giving a first-order rate coefficient for HONO loss of roughly $1 \times 10^{-4} s^{-1}$. This loss process reproduces observations modestly better than the assumption that NO_2 conversion is much slower than has been previously reported (Figures S5 and S6). The near steady state in HONO/NO_2 near the surface observed at NACHTT-11 is also consistent with vertical profiles measured by *Wong et al.* [2011] in the urban atmosphere of Houston, Texas, and with other studies over land [*Kleffmann et al.*, 2003; *Stutz et al.*, 2004] and the ocean [*Wojtal et al.*, 2011]. However, the use of HONO/NO_2 to calculate HONO formation rates at night during this observation period is not possible.

[21] The utility of HONO/NO_2 to estimate formation rates of HONO at night implies that there are no other significant losses of NO_2. However, under low temperature conditions, such as those found in the winter, other loss process of NO_2 must be considered. The equilibrium formation of N_2O_5 from

NO_3 and NO_2 (R6, R7), favored at low temperatures and high NO_x, may impact the ratio of HONO to NO_2. In order to examine this effect, we consider the ratio of HONO to the sum of NO_2, NO_3, and N_2O_5.

$$NO_{2(g)} + O_{3(g)} \rightarrow NO_{3(g)} + O_{2(g)} \qquad (R6)$$

$$NO_{3(g)} + NO_{2(g)} \rightleftharpoons N_2O_{5(g)} \qquad (R7)$$
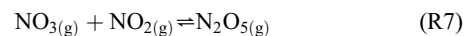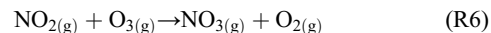
[22] Figure 4 shows that the difference between the ratios HONO/NO_2 and HONO/(NO_2 + NO_3 + (2*N_2O_5)) grew as the night progressed. At any given time, these two ratios became indistinguishable near the ground. Four chemical processes may help explain the observations made during NACHTT-11: (i) deposition of HONO at the ground surface, (ii) increased emissions of NO_2, (iii) a competing sink of NO_2 reacting with O_3 (R6) aloft, and (iv) fast loss of NO_3 and N_2O_5 at the ground surface. Near the surface (roughly, 0–50 m AGL) in Figure 4, there are clear decreases in HONO/NO_2 as the profiles transition from the residual layer to the NBL (20–22, 02–04, and 04–06 h) consistent with a loss term for HONO and/or a production term for NO_2. The increasing difference between HONO/NO_2 and HONO/(NO_2 + NO_3 + (2*N_2O_5)) above the NBL demonstrates that an increasingly large fraction of reactive nitrogen is present as N_2O_5 aloft. Loss rates of NO_2 to form NO_3 (R6) above the NBL are on the order of 5 times faster than at the surface because of higher O_3 mixing ratios and temperatures aloft, where formation of NO_3 is 5–25 times faster than NO_2 uptake to surfaces (section E in the supporting information). Therefore, the observed increase of HONO/NO_2 with increasing height within 50 m of the surface could be due to: (i) formation and heterogeneous losses of NO_3 and N_2O_5, (ii) HONO deposition to the ground, and (iii) NO_2 emissions at the surface. From this analysis, it was not possible to explicitly identify the process(es) responsible. In particular, observable products of NO_2 loss processes at the surface are reduced because reagent concentrations are lower, and NO_3 and N_2O_5 are lost rapidly through heterogeneous uptake [*Brown et al.*, 2007; *Chang et al.*, 2011]. Therefore, the use of either ratio may not be the best parameterization for understanding winter HONO production at the surface. In this data set, explicit vertical information on HONO, NO_2, and submicron aerosol surface area are available to directly constrain HONO production and loss.

[23] Under the assumption that HONO deposition back to the surface is responsible for the near steady state observations in our chemical model, the potential quantity of HONO deposited to the surface is significant in comparison to the calculated/inferred deposition of HNO_3 over the course of a night (~40%, Figure S5). Assuming that ground surface production and loss dominate observed HONO mixing ratios at night, the integrated column amount of HONO can be described in terms of surface processes, which is explored in more detail in section 3.1.4. This new approach directly evaluates HONO production rather than assume that HONO/NO_2 is an effective proxy, which could be misleading for this data set.

3.1.3. Relative Importance of Aerosol and Ground Surface in Nocturnal HONO Production

[24] The uptake coefficients required to explain nocturnal heterogeneous HONO production from reaction of NO_2 on submicron aerosol surface were evaluated against the best

available constraints on reactive uptake coefficients of NO_2 from the model of *Wong et al.* [2011] and lab studies on NO_2 uptake and conversion [*Bröske et al.*, 2003; *Kleffmann et al.*, 1998; *Kurtenbach et al.*, 2001]. The yield of the hydrolysis reaction assumed equimolar disproportionation of two NO_2 molecules to form HONO and HNO_3, immediately releasing HONO [*Finlayson-Pitts*, 2009; *Finlayson-Pitts et al.*, 2003]. Aerosol reactive uptake of NO_2 was assumed to occur on all measured (submicron) surface area, regardless of chemical composition, using the reactive uptake approximation of *Fuchs and Stugnin* [1970] for submicron aerosols and small uptake coefficients (equation (1)), modified to account for the disproportionation.

$$P_{(HONO)} = \frac{1}{2} \frac{\gamma_{NO_2} A \sqrt{3RT/M}}{4} [NO_2] \qquad (1)$$

where γ is the uptake coefficient, and A is the hydrated aerosol surface area ($\mu m^2\,cm^{-3}$). The gas constant ($R = 8.314\,J\,mol^{-1}\,K^{-1}$), temperature ($T$, K), and molecular mass of NO_2 ($M = 4.6 \times 10^{-2}\,kg\,mol^{-1}$) are used to calculate molecular speed.

[25] An estimate of the γ_{NO_2} required to account for observed HONO production was made using hydrated submicron aerosol surface area and NO_2 observations from the residual layer, since we can expect it to be decoupled from the ground and largely free of NO_2 emissions. The surface area of supermicron aerosol was not quantified during NACHTT but is generally smaller than submicron areas [*Aldener et al.*, 2006], despite the nontrivial quantities observed [*Young et al.*, 2013]. Therefore, this is a lower limit estimate of the total surface area for the heterogeneous reaction. The approximation was made using an upper limit of observed nocturnal NO_2 in the residual layer of 5 ppbv, a representative temperature of 273 K, and an aerosol surface area of $60\,\mu m^2\,cm^{-3}$, typical of the residual layer. A mixing ratio of 5 ppbv of NO_2 would require an uptake coefficient of 3×10^{-4} to 8×10^{-4} to account for typical 2 h increases of 30–60 pptv HONO. The absolute amount produced in an interval of 2 h would barely be observable relative to the variability between profile measurements, which was ±50 pptv (Figure 4). Exaggerating the comparison to 15 ppbv of NO_2, and $100\,\mu m^2\,cm^{-3}$ submicron aerosol surface area (typical values within the NBL), the uptake coefficient would need to be at least 1.17×10^{-4} to produce 30 pptv of HONO in 2 h, and such high values of NO_2 or submicron aerosol were seldom observed in the residual layer (Figure 2). These NO_2 uptake coefficient values are a factor of 12–875 greater than those observed in studies on relevant surfaces, which ranged between 1×10^{-6} to 1×10^{-5} [*Kleffmann et al.*, 1998; *Kurtenbach et al.*, 2001]. If we assume that lab-derived coefficients are accurate, and NO_2 were converted to HONO only on aerosol surfaces, the absolute amount produced in an interval of 2 h would barely be observable relative to the variability between vertical profile measurements (±50 pptv HONO; Figure 4). Thus, production solely on aerosols cannot explain HONO observations during NACHTT.

[26] Taken together—high correlation between HONO and NO_2 in the nocturnal boundary layer, highest HONO mixing ratios at the surface, insufficient aerosol surface area to account for observed HONO production, and near steady state of HONO/NO_2—all suggest that HONO observed throughout the depth of the NBL is primarily derived from heterogeneous conversion of NO_2 on the ground followed by vertical transport throughout the column. Measurements of these chemical species and physical parameters throughout the NBLs encountered during NACHTT-11 can, therefore, be used to directly constrain the range of values for both NO_2 and HONO uptake coefficients at the ground surface.

3.1.4. Observationally Constrained Ground Surface Uptake Parameters for NO_2 and HONO

[27] Nocturnal surface production of HONO was parameterized based on the assumption that production of HONO on aerosols was insignificant compared to the ground surface, which has been suggested in other studies of HONO vertical structure [*Villena et al.*, 2011; *Wong et al.*, 2011; *Zhang et al.*, 2009]. During NACHTT-11, it was possible to evaluate the rate of change of HONO in the atmospheric column as a function of HONO and NO_2 number densities in contact with the surface using their integrated, bihourly averaged, NBL column densities. Surface transport processes for reactive gases are a consistent feature of vertically resolved model runs by *Wong and Stutz* [2010] and *Wong et al.* [2011] where the transport of NO_2 and HONO to the surface must be calculated to compare to measurements. In contrast, here we constrain a model with direct observations of surface production and loss of these gases (see section 3.3). At night, the change in integrated HONO throughout the column was parameterized as a function of NO_2 and HONO concentrations measured near the ground surface, which can be approximated using the mean molecular speed (C) of the respective gases as shown in equation (2).

$$\frac{dHONO_{column}}{dt} = \frac{1}{8} \gamma_{NO_2,ground} C_{NO_2} [NO_2]_{ground}$$
$$- \frac{1}{4} \gamma_{HONO,ground} C_{HONO} [HONO]_{ground} \qquad (2)$$

where $dHONO_{column}/dt$ is the observed change in NBL column-integrated surface density of HONO (molecules cm^{-2}), and $[NO_2]_{ground}$ and $[HONO]_{ground}$ are the average number densities of NO_2 and HONO measured within 1–10 m of the ground, assuming that measurements between these heights are representative for the surface. The second term in equation (2) determines the net exchange of HONO from the vertically resolved observations and does not assume irreversible loss to the surface. In addition to high correlations ($R^2 \geq 0.8$) between HONO and NO_2 throughout the NBL (Figure S4), if the production of HONO at night is indeed dominated by reactions at the ground surface, the integrated column concentration of HONO is expected to show proportionality to the amount of HONO observed at the surface. Figure 5 shows that the integrated column of HONO is related to the amount of HONO observed between 1 and 10 m ($R^2 = 0.66$), which is consistent with the ground surface being the location where HONO is predominantly formed.

[28] Nearly all of the HONO produced at the surface remains in the lowest 250 m of the atmosphere on nights with NBLs, so the observed rates of change in the total column HONO can be used to investigate ground sources and sinks without explicitly considering the meteorology or vertical mixing. The ground uptake coefficient of NO_2 was solved for using observations collected between 18:00 and 24:00 MST, when HONO mixing ratios were small, typically below
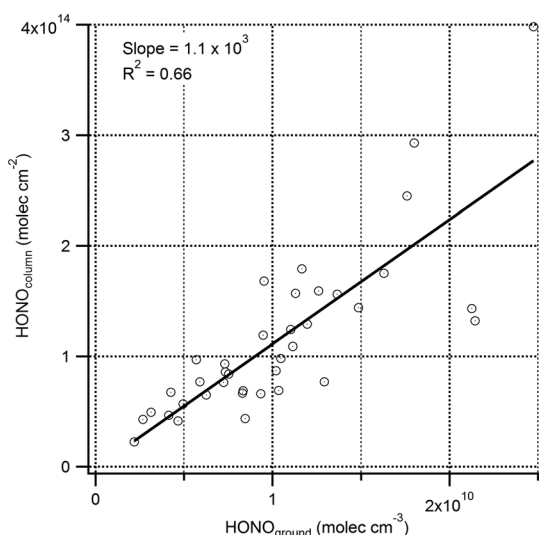
Figure 5. Orthogonal linear least squares correlation between 2 h average total NBL column HONO and HONO measured from the surface to 10 m AGL. Column values were calculated for the nine nights at the BAO tower with identifiable NBLs (i.e., integrated HONO surface density was quantified to the top of the identified thermal inversion layer) indicating surface formation as an important source of nighttime HONO.

250 pptv, by setting the left-hand site of equation (2) equal to the first term on the right-hand side.

[29] Figure 6 displays the relationship between observed HONO column density increases and the NO_2 number density between 0 and 10 m, used to calculate the uptake coefficient. Nights with distinct NBLs yielded a range of uptake coefficients for NO_2 at the surface ($\gamma_{NO2,\ ground}$) for the total column production of HONO. The ground uptake coefficient for NO_2 determined from the best linear least squares fit to the data in Figure 6 (i.e., $\gamma_{NO2,\ ground} = 8*$ slope/C_{NO2}) was 8.0×10^{-6}. The average coefficient calculated from all individual data points was $8.0 \pm 1 \times 10^{-6}$, with the range spanning values between 2×10^{-6} and 1.6×10^{-5}. These values are all within the range of reactive uptake coefficients of NO_2 on surfaces (1×10^{-6} to 1×10^{-5}) determined by several lab studies [*Bröske et al.*, 2003; *Kleffmann et al.*, 1998; *Kurtenbach et al.*, 2001]. For a constant amount of NO_2, the amount of HONO produced increases with relative humidity, particularly at values greater than 50% (Figure 6). Conversion of NO_2 to HONO according to (R2) requires adsorbed water at a surface for the reaction to proceed, and these results are consistent with previous observations [e.g., *Stutz et al.*, 2004] that HONO production increases with relative humidity for a constant amount of surface NO_2.

[30] The relative humidity dependence of HONO formation has been suggested by numerous lab studies [*Finlayson-Pitts*, 2009; *Finlayson-Pitts et al.*, 2003; *Miller et al.*, 2009; *Ramazan et al.*, 2006]. The dependence on HONO formation as a function of relative humidity from field data has been addressed by *Stutz et al.* [2004] and recently revisited by *Wojtal et al.* [2011]. *Stutz et al.* [2004] found an increased likelihood of a higher ratio of HONO to NO_2 at high relative humidities, in particular, suggesting that HONO production was often enhanced at relative humidities above

60%, similar to the NACHTT-11 observations made at the BAO tower. Based on these previous observations and the data shown in Figure 6, we parameterized the NO_2 uptake coefficient for a chemical model (section 3.4) by applying a factor of RH/50 to the first term in equation (2) as the lower and upper bounds of the range were roughly factors of 2 smaller and larger than the average coefficient calculated (equation (3)).

[31] Between midnight and sunrise (00:00–06:00), the deposition of HONO becomes an increasingly important term in equation (2) as the absolute amount of HONO grows. Equation (2) was used to solve for the HONO sink term using the relative humidity dependent parameterization of $\gamma_{NO2,\ ground}$ to estimate the deposition rate of HONO to the surface. The difference between the calculated column rate of production and the observed column rate of change for 2 h intervals between 0:00 and 06:00 MST is plotted against the observed HONO in Figure 7. This approach yielded $\gamma_{HONO,\ ground}$ uptake coefficients of 8.7×10^{-5} from fitting the data with a linear least squares regression, and $7.3 \pm 1 \times 10^{-5}$ averaged from all data points, covering a range from 2.0×10^{-5} to 2.0×10^{-4}. These calculated uptake coefficients are roughly an order of magnitude larger than $\gamma_{NO2,\ ground}$ and consistent with the relative magnitudes for these terms employed in models of nocturnal production and deposition by *Wong et al.* [2011]. Furthermore, the data in Figure 7 suggest that there may also be relative humidity dependence to the uptake of HONO on the ground surface. We parameterized this by a factor of RH/20 applied to the second term in equation (2) through observation that the uptake coefficient of HONO increased with RH by a factor of 2.5 more than for NO_2 (data
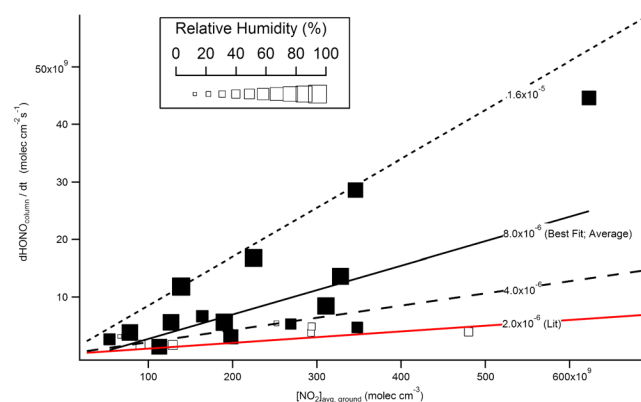

Figure 6. Surface dependence for reaction of NO_2 on the ground in the production of HONO throughout the observed atmospheric column at BAO tower for the nine nights with identifiable NBLs from 18:00 to 00:00 MST. HONO$_{column}$ values were integrated from the surface to the NBL, and $NO_{2,surface}$ concentrations were averaged from the surface to 10 m AGL. Lines on graph indicate the effective $\gamma_{NO2,\ ground}$ from (i) orthogonal linear least squares analysis (solid black, 8.0×10^{-6}), (ii) double the best fit (short dash, 1.6×10^{-5}), (iii) value derived from NO_2 0.02 cm s^{-1} deposition velocity of *Spicer et al.* [1989] (solid red, 2.0×10^{-6}), and (iv) half of best fit (long dash, 4.0×10^{-6}). Marker sizes represent relative humidity, open squares indicate relative humidities below 50%, and filled squares above 50%.
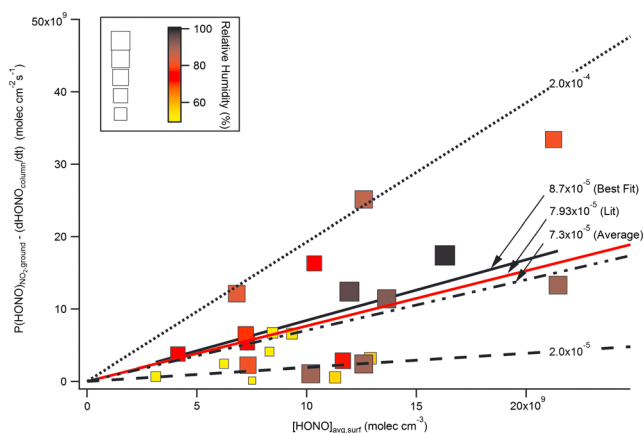
Figure 7. Production of HONO from the reaction of NO_2 on the ground surface in excess of the observed change in column HONO as a function of the average HONO observed at the surface between 00:00 and 06:00 MST. The slope of the orthogonal linear least squares analysis is the product of $\gamma_{HONO,ground}$ and the mean molecular speed of HONO (C_{HONO}). The values displayed for each line are the effective $\gamma_{HONO,ground}$ for (i) linear fit to observed data (solid black, 3.2×10^{-5}), (ii) average calculated value (dash-double dot, 2.3×10^{-5}), (iii) upper limit of observed data (dotted, 5×10^{-5}), (iv) best fit when $\gamma_{NO2,ground}$ used from *Spicer et al.* [1989] (solid red, 1.8×10^{-5}), and (v) lower limit of observed data (dashed, 2.0×10^{-5}). The color scale and marker size denote relative humidities.

not shown). We can use these results to update the term in equation (2), for use in a chemical model (section 3.4):

$$\frac{dHONO_{column}}{dt} = \frac{1}{8}\gamma_{NO_2,\,ground}\frac{RH}{50}[NO_2]_{ground}C_{NO_2}$$
$$-\frac{1}{4}\gamma_{HONO,\,ground}\frac{RH}{20}[HONO]_{ground}C_{HONO} \quad (3)$$

[32] Partitioning of HONO to simulated dew has been studied in a flow tube by *He et al.* [2006]. The uptake loss is also pH dependent and has been observed or suggested in several investigations [*Becker et al.*, 1998; *He et al.*, 2006; *Hirokawa et al.*, 2008; *Kleffmann et al.*, 1998; *Longfellow et al.*, 1998], as would be expected for a weak acid. Therefore, parameterization of the HONO surface deposition will likely change between environments depending on the dominant characteristics of the surface on which NO_2 reacts to form HONO and the subsequent capacity of the surface to also act as a HONO sink. The BAO tower was surrounded by grassland and tilled earth, the latter with a measured pH of 7.7 for a local soil sample (in a 50:50 slurry with deionized water), where the effective partitioning coefficient of HONO would be high ($K_{eff} = 6.4 \times 10^5$ M atm^{-1}). Urban or forested areas have buildings, paved, and plant surfaces that are expected to change the deposition efficiency of HONO. Furthermore, the approach taken here describes the net effect of HONO exchange at the surface, as emission of HONO directly from a reservoir such as soil pore water nitrite [*Su et al.*, 2011] cannot be excluded from this analysis. These field-derived surface parameters of nocturnal HONO

production from NO_2 and surface deposition of HONO are consistent with the modeling estimates of these processes for observations made in Houston, Texas, by *Wong et al.* [2011].

[33] A simple resistance model, following *Huff and Abbatt* [2002], estimating transport, diffusion, and reactive losses operating in series at the surface, was used to determine the factor(s) controlling the potential broad scale applicability of the γ-coefficients calculated here for the uptake of NO_2 and loss of HONO. The details of this analysis are presented in section E of the supporting information (Figure S5). The results indicated that HONO surface uptake coefficients from 2×10^{-5} to 2×10^{-4} are potentially limited by a combination of transport and diffusion to the ground surface if the real uptake coefficients are greater than 2×10^{-4}. However, if the reactive uptake coefficient of HONO is closer to 2×10^{-5}, the system will be limited by reaction probability at the surface, except at wind speeds less than $2\,m\,s^{-1}$. A combination of transport, diffusion, and reaction processes was likely observed during NACHTT-11, suggesting that these values represent a lower limit on the uptake coefficient of HONO on the ground surface.

[34] Conversely, the range of NO_2 uptake coefficients ($\gamma_{NO2,\,ground} < 1.6 \times 10^{-5}$) indicates limitation only by the reactive uptake process. The broad scale applicability of these field-derived terms for surface conversion of NO_2 should therefore be possible, while those found for HONO ($\gamma_{HONO,\,ground} = 2 \times 10^{-5}$ to 2×10^{-4}) require further exploration from controlled lab studies. More observations from various environments are required to enable models to better predict the extent of HONO deposition and the variability of these nocturnal processes. The consistency between our findings, investigations of NO_2 conversion on wet surfaces, and the values of these parameters in models suggest that the calculated coefficients are within the appropriate order of magnitude of their true values.

3.2. Daytime HONO

[35] Vertical profiling was interrupted during the daytime for instrument maintenance, resulting in only 6 days with near-continuous vertical profiles from 06:00 to 18:00 MST. Throughout the day, HONO was observed above the 3.8 pptv detection limits of the NI-PT-CIMS throughout the 250 m profiles, with average daytime minimum mixing ratios of 100 ± 80 pptv at the surface and 35 pptv aloft. Figures 2 and 8 show the characteristic diurnal cycle as HONO formed from the previous night undergoes photolysis throughout the column during the early morning hours, mixes throughout the boundary layer around 10:00, and continues to decrease throughout the column for the duration of the day, eventually reaching a steady state (i. e., dHONO/dt ≈ 0) throughout the observed column between 14:00 and 18:00.

[36] Average daytime mixing ratios of 100 ± 80 pptv HONO observed between 12:00 and 16:00 MST throughout the campaign were higher compared to the expected range of 10 to 25 pptv based on the balance of calculated HONO photolysis and gas phase production and loss (R1, R3, and R5). Vertical profiles during the day also showed HONO enhanced near the surface (Figure 8). Both of these observations are indicative of a daytime HONO surface source. Although lab-derived mechanisms for HONO production at the ground surface are not well-constrained by field observations due to the
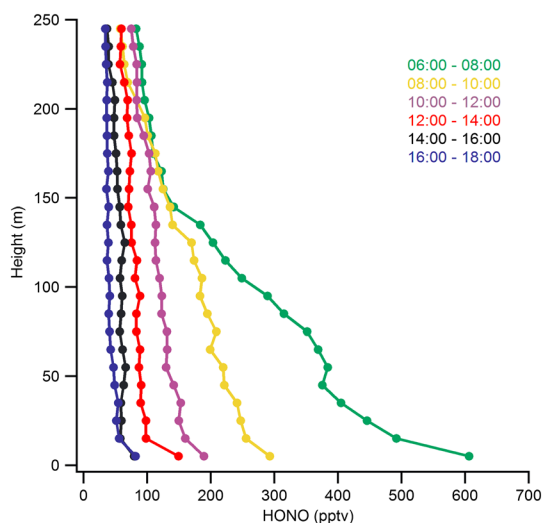
Figure 8. Average vertical profiles of daytime HONO from all daytime measurements made during NACHTT-11 at 10 m intervals, starting at 5 m AGL. Each trace represents a 2 h average of vertical HONO measurements decreasing throughout the course of the day.

difficulty in quantifying their separate contributions, the potential HONO production from these sources has been considered too small (at most 30%, but often not quantified) to account for daytime HONO production rates in polluted regions, where the required source strength ranges from ∼0.2 to 2 ppbv h^{-1} [*Kleffmann*, 2007; *Kleffmann et al.*, 2005; *Qin et al.*, 2009; *Sörgel et al.*, 2011b; *Su et al.*, 2008a; *Wong et al.*, 2012]. We return to this issue in section 3.3.

[37] Daytime vertical profiles of HONO measured by differential optical absorption spectroscopy in Houston, Texas, have also found evidence that the ground surface is a HONO source during daytime [*Wong et al.*, 2012]. In the NACHTT data, there are obvious discontinuities between the lowest two heights (5 and 15 m) of each 2 h average profile which were observed on all days (Figure 8). Fine-scale gradient measurements of daytime HONO showing this

structure have not been previously reported. These observations are consistent with the hypothesis that daytime production of HONO is consistently occurring at the ground surface and being mixed throughout the daytime boundary layer.

3.3. Evidence for Nocturnally Deposited HONO as a Daytime Source

[38] Given our observational evidence that the ground surface acts as a sink of HONO during the night and a source during the day, we hypothesize that the ground surface may form a reservoir whose re-emission can act as a HONO source the following day.

[39] To the best of our knowledge, this potential daytime source has not yet been addressed in the literature. Several model scenarios were explored to determine the relative quantities of HONO produced on and deposited to the ground surface at night according to values obtained from the literature and those derived in this study. The magnitude of this term was then compared to the calculated total daytime HONO production from the unknown source.

[40] The chemical box model, shown in equation (4), was used to separate the contributions of individual chemical processes involved in the diurnal production and loss of HONO throughout the measured column (details in the supporting information), including the unknown daytime source strength (P(HONO)$_{unk}$) required to reconcile observations with known processes. The constraints on this model are measurements made at, or below, a fixed height of 20 m AGL.

$$\frac{d[HONO]}{dt} = P(HONO)_{unk} + k_3[OH][NO] + \frac{1}{8}\frac{\gamma_{NO_2,ground}C_{NO_2}}{h}[NO_2]_{ground}$$
$$- \frac{1}{4}\frac{\gamma_{HONO,ground}C_{HONO}}{h}[HONO]_{ground} - k_5[HONO][OH]$$
$$- j_{HONO}[HONO]$$

(4)

[41] The surface production of HONO via NO$_2$ and subsequent loss back to the surface, both terms in equation (3), were used as more accurate representations of nocturnal production and loss of HONO in equation (4). When the vertical structure and integrated column changes in HONO and NO$_2$
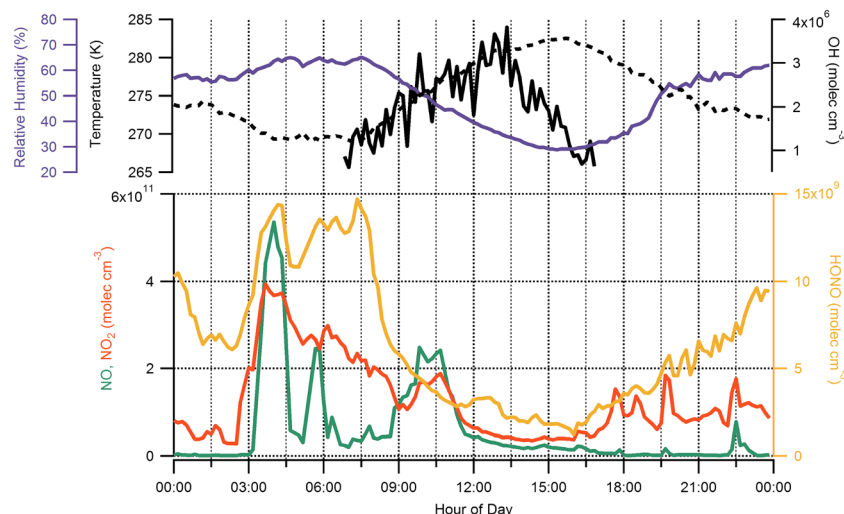

Figure 9. Box model input values of measured constraints (0–20 m AGL) from 18 to 27 February 2011 for diurnal modeling of HONO chemical behavior and quantifying the missing HONO source/sink.
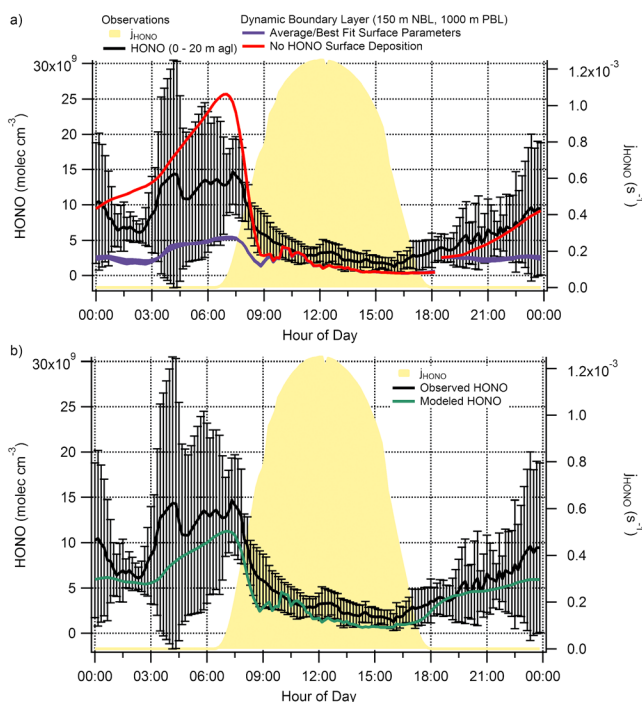
Figure 10. Observed HONO atmospheric concentrations (left axis, black line, ±1σ) and the calculated HONO photolysis rate (right axis, filled yellow) from 19 to 25 February during NACHTT-11 from 0 to 20 m AGL. (a) Modeled HONO production throughout the mixed boundary layer is determined from observational constraints with field-derived surface exchange parameters for the NO₂ heterogeneous reaction (R1) without depositional loss of HONO (red line) and with depositional loss of HONO (blue line) included in the calculation of boundary layer HONO concentrations and (b) predicted HONO number density at 20 m AGL when depositional HONO loss (green line) is included in model.

are not known, the more traditional approach is to use NO_2 conversion frequencies (0.1% to 2%) [*Sörgel et al.*, 2011b; *Su et al.*, 2008a]. Model scenarios representing the reactions of NO_2 and HONO with and without relative humidity dependence on the ground surface were used to explore the relative magnitudes of nocturnal surface-deposited HONO and the integrated unknown daytime HONO source.

[42] A comparison between our HONO heterogeneous production term and a literature dry deposition velocity of NO_2 to the surface, V_{dep}, of $0.02 \, cm \, s^{-1}$ [*Spicer et al.*, 1989] in a boundary layer of height, h, was made by inserting equation (5) in place of $\frac{1}{8} \gamma_{NO_2,ground} C_{NO_2}$.

$$P_{(HONO)} = \frac{1}{2} \frac{V_{dep, NO_2}}{h} [NO_2] \quad (5)$$

[43] Horizontal and vertical advection were not explicitly represented in this model but were assumed to be reasonably captured by the column-integrated rate of change of HONO measurements (i.e., the advection terms are similar over a wide area). It was also assumed that the well-mixed daytime boundary layer was not significantly influenced by direct HONO emissions from local point sources and that conditions observed

at the tower represent those of the local area. Chemical production of HONO in the model was initialized at 18:00 MST using the diurnally averaged 10 min observations from Figure 9 collected between 18 and 27 February 2012. The model trials were limited to this time period by the duration of available OH measurements.

3.4. Magnitude of Nighttime HONO Deposition and the Daytime Surface HONO Source

[44] Figure 10a shows several model scenarios of HONO sources and sinks, while Figure 10b depicts a representative set of model conditions compared to the range of observations made over 0–20 m AGL. Nighttime production and loss is distinct from the daytime, and we discuss the nighttime first. In the case where nocturnal production of HONO at the surface occurs without any loss processes, the predicted HONO number density grows continuously throughout the night, strongly overestimating HONO concentrations (Figure 10a, red trace). The observations, as discussed above, show a similar increase early in the night, but then reach an approximate plateau after midnight in which there is variability but no trend. This comparison implies that there is a significant HONO sink in the nocturnal boundary layer (i.e., deposition to the ground) that approximately balances the production term late in the night.

[45] When RH-dependent surface parameters derived from the column HONO and NO_2 observations on nine nights with NBLs (equation (4)) are implemented in the model (Figure 10a, blue trace), the late night plateau is reproduced, indicating that surface loss of HONO is an important sink to consider. The data set to which the RH-dependent surface parameters are applied with this model contains two of the nights from which they were derived and four others. Therefore, the general description in equation (4) seems to accurately capture the processes of HONO formation and loss at the ground surface at night. Note that the underestimation of the HONO concentration output by the model when using a 150 m nocturnal boundary layer compared to the observations made at 20 m are expected due to the increase in HONO concentration as the surface is approached (i.e., the presence of vertical gradients). Also note that the specific uptake coefficients most likely have variability that is difficult to completely capture in a simple parameterization. This model was tested for sensitivity toward the relative humidity parameterization developed (i.e., equation (2) versus equation (3)), but this case study was found to affect the calculated HONO concentrations minimally (i.e., width of blue trace, Figure 10a). This negligible influence is not surprising given the low relative humidities and small diurnal variation in relative humidity (30%–60%) for this period (Figure 9).

[46] The two surface parameters for NO_2 and HONO in equation (4) were rerun in a final case with a surface layer depth of 20 m AGL and compared with observations (Figure 10b; green trace). This captures the nighttime HONO production within 30%, which is within the variability of measured values. The agreement supports the observation-based hypothesis that HONO nocturnal chemistry is dominated by the ground surface, as our model does not require any aerosol NO_2 conversion. The lower concentrations calculated throughout the night indicate that the parameterization of the source and sink terms need to be investigated more explicitly in future lab
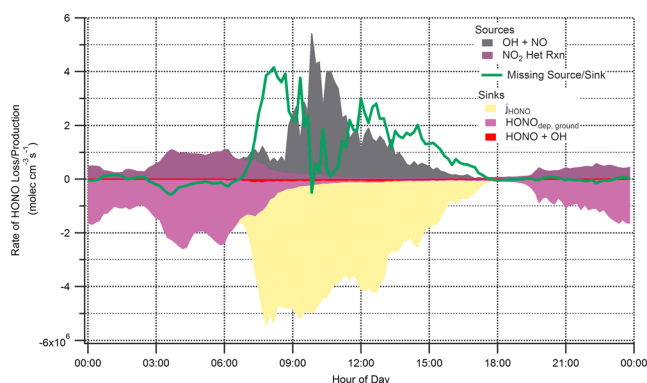
Figure 11. Separated contributions of $P(\text{HONO})_{\text{unk}}$ in the chemical model throughout the mixed layer for 19–25 February 2011. Relative and overall magnitudes are shown by stacking sources (positive) and sinks (negative). The model run calculated the missing source using observational constraints on NO_2 ground conversion (8.0×10^{-6}) and HONO reactive loss (7.3×10^{-5}) from vertical profiles during NACHTT-11. The calculated missing source/sink of HONO is overlaid (green line).

and field studies. Figure 11 depicts the modeled HONO sources and sinks, displayed as stacked terms.

[47] The conversion of NO_2 on the ground surface is the most important source of HONO throughout the night. The rural location of the BAO tower is surrounded largely by grassland and tilled farms. Soils are characterized by a persistent surface water layer under atmospherically relevant conditions of temperature and relative humidity [*Conklin*, 2005], which would allow for NO_2 heterogeneous reaction throughout both night and day. However, the magnitude of this source is clearly underestimated in our model since HONO production is less than HONO loss at this interface, when HONO is known to be accumulating in the NBL. The observational constraints from the field, however, ensure that the total HONO does increase in the model. As described earlier, the surface loss of HONO is also poorly constrained and may be smaller during the modeled period than the average value for the campaign. Furthermore, the relative humidity weighting from equation (4) was applied in a linear fashion based on a best representation of the data from this study. However, the conversion of NO_2 [*Stutz et al.*, 2004] and uptake of HONO on wet surfaces may, in reality, be nonlinear and not described so simply. Overall, the accuracy in this parameterization to within 30% of the measured values is good, given the lack of meteorological terms in the chemical model, the variability in the observations during the comparison period, and the uncertainty in the measured levels of gas phase species (i.e., OH (35%), HONO (17%), NO_2 (5%), and NO (5%)).

[48] The discrepancy between modeled and observed HONO during the day is indicative of a daytime surface source of HONO. Production of HONO from gas phase chemistry between OH and NO during the day dominates and was particularly significant when plumes of fresh NO_x emissions were intercepted at this site (Figure 11). The loss of HONO by photolysis is the dominant sink of HONO during the day, with minor contributions from surface deposition in the morning and negligible loss to OH. In all cases, from

09:00 to 17:00, the model photostationary state undercalculates the observed steady state minimum in HONO, except for a short period from 10:00 to 11:00. The discrepancy between these daytime sources and sinks is assumed to be equal to additional missing source(s) of HONO $(P(\text{HONO})_{\text{unk}})$ in order to account for the observed atmospheric concentration of HONO. The same case studies as described above for nighttime data were used to explore the implied daytime HONO source strength. The magnitude of the missing HONO source was calculated for the period 19–25 February using averaged 10 min resolution measurements from 0 to 20 m, by solving for $P(\text{HONO})_{\text{unk}}$ in equation (4), and is overlaid as a green line in Figure 11. The unknown source of HONO is highest in the morning $(4 \times 10^6 \text{ molecules cm}^{-3}\text{ s}^{-1},\ 600 \text{ pptv h}^{-1})$ and declines throughout the day to about 1×10^6 molecules cm^{-3} s^{-1} (165 pptv h^{-1}). The daytime source at BAO during the winter is consistent with the range of strong daytime HONO surface sources determined at other field locations, with source strengths ranging from 100 to 1000 pptv h^{-1} [*Amoroso et al.*, 2008; *Elshorbany et al.*, 2009, 2012; *Kleffmann*, 2007; *Kleffmann et al.*, 2005; *Qin et al.*, 2009; *Sörgel et al.*, 2011b; *Su et al.*, 2008a].

[49] The modeled period of near-continuous observations from 19 to 25 February in Figure 9 (observations) and Figure 10 (model) shows that the arrival of local NO_x plumes between 09:00 and 12:00 in the morning significantly increases the predicted HONO production. The NO reaction with the observed levels of OH results in a significant reduction in the unknown source strength of HONO required to balance the model. This potentially indicates that the daytime HONO source strength at the surface depends on the HONO concentration in the overlying atmosphere. That a continuous source was not observed during this period suggests that the system may be more dynamic than previously considered. It has been shown by *Wong et al.* [2012] that $P(\text{HONO})_{\text{unk}}$ normalized to NO_2 correlates strongly to the total surface irradiance. In this case, if photochemical mechanisms were the dominant source of the unknown HONO, they would be expected to be enhanced, not suppressed, in the presence of additional NO and NO_2 (Figures 9–11). The magnitude of the daytime HONO source here is similar to that observed in summertime campaigns and exhibits a similar trend in $P(\text{HONO})_{\text{unk}}$ [*Wong et al.*, 2012]. Therefore, the daytime HONO source at the BAO tower during winter may arise from an alternative mechanism, such as a reservoir of HONO generated at the ground surface, or in the soil, throughout the night that is released during daytime. The fate of HONO deposited at night has not been previously explored, but the decreasing trend in $P(\text{HONO})_{\text{unk}}$ throughout the day is consistent with the depletion of a surface HONO reservoir.

[50] Proposed mechanisms for daytime HONO formation have largely been based on the conversion of NO_2 on a photoexcited surface. The observations of *Wong et al.* [2012] show that this mechanism is likely active during the day, but its significance has not yet been compared to other processes on a mass basis. A recent study by *Sörgel et al.* [2011b] has suggested that the largest contributing photocatalytic mechanism is humic acid conversion of NO_2, approximated at 30% of the daytime source for a semi-urban location in Spain. Furthermore, NO_2 and surface irradiance are expected to show an anticorrelation as NO_2 is diluted and lost during the day. Correlation between $P(\text{HONO})_{\text{unk}}/NO_2$ and surface irradiance
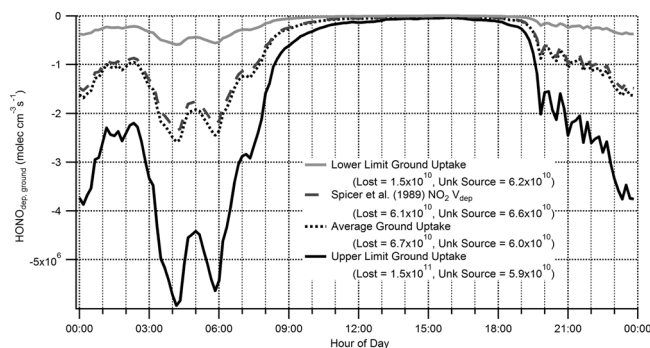
Figure 12. Overlaid temporal loss rates of HONO by relative humidity dependent ground uptake (E3) parameterized by four approaches from lines in Figures 9 and 10: (i) lower limit of NO$_2$ and HONO surface reactions (grey, solid line), (ii) upper limit of NO$_2$ and HONO surface reactions (black, solid line), (iii) average ground uptake (black, dotted line), and (iv) literature comparison of NO$_2$ deposition velocity from *Spicer et al.* [1989] (grey, dashed line). Integrated daily loss of HONO (Lost) and the integrated unknown source of HONO (Unk Source) under each set of parameterizations are provided in molecules cm^{-3} d^{-1}.

is expected if P(HONO)$_{unk}$/NO$_2$ is nearly constant throughout the day, as was observed at the BAO tower and in Houston [*Wong et al.*, 2012]. Consequently, using a ratio approach to understand daytime HONO production may be misleading unless the assumption that conversion of NO$_2$ is the sole source of HONO can be demonstrated as reasonable.

[51] Investigations of alternative HONO sources, not requiring NO$_2$, need to be conducted and contrasted to existing mechanisms to elucidate the relative importance of NO$_2$ as a daytime HONO precursor against potential HONO reservoirs. Recently, soil nitrite has been proposed as a potential daytime source of HONO via a dynamic equilibrium regulated by soil water content, pH, and overlying composition of the atmosphere [*Su et al.*, 2011], similar to a traditional NH$_4^+$/NH$_3$ compensation point. Also, the photolysis of HNO$_3$ on surfaces has been postulated as a potential source of HONO [*Zhou et al.*, 2003, 2011; *Ziemba et al.*, 2010]. Both soil nitrite and surface nitrate represent potential reservoirs for daytime HONO which are not dependent on the ambient NO$_2$. Our data are inconsistent with both soil nitrite and HNO$_3$ photolysis, the former being temperature dependent and the latter being sunlight dependent, neither of which were observed to follow P(HONO)$_{unk}$. The data presented in Figures 11 and 12 show that a significant amount of HONO could be deposited to the surface during the night, possibly forming a reservoir. The fate of HONO or nitrite deposited on the ground is not known, but loss processes may occur. As such, our assumption that HONO deposited to the surface is conserved should be noted and our estimates viewed as upper limits for its capacity. We explored the relative magnitude of the integrated loss of HONO to the surface and the integrated HONO source strength by testing the sensitivity of the model reservoir to the range of γ$_{HONO, ground}$ values found from the integrated HONO column measurements.

[52] Total HONO produced by the unknown daytime source, within 20 m AGL, during NACHTT-11 ranged from 5.9×10^{10} to 6.6×10^{10} molecules cm^{-3} d^{-1} for the period of 19–25 February. The nighttime depositional losses of HONO

derived from the range of surface uptake coefficients were more variable, ranging from 1.5×10^{10} to 1.5×10^{11} molecules cm^{-3} d^{-1}. The uncertainty in the calculated γ$_{HONO, ground}$ does not depend strongly on the assumptions made about γ$_{NO2, ground}$. Even when using the literature reported value of $V_{dep, NO2} = 0.02$ cm s^{-1} (γ$_{NO2, ground} = 2.0 \times 10^{-6}$ [*Spicer et al.*, 1989]), γ$_{HONO, ground}$ still falls within the range observed (Figure 7; red line). The parameterization of γ$_{HONO, ground}$, therefore, is likely accurate within a factor of 2 and well represented by the average coefficient (7.3×10^{-5}). In Figure 12, the influence of the γ$_{HONO, ground}$ coefficients on the magnitude of the total HONO deposited to the ground surface is presented. In three out of four cases, the HONO deposited to the ground was sufficient to explain the daytime source with values of 93%, 112%, and 250% of the integrated daytime source calculated. Using the absolute lower limits for NO$_2$ conversion and HONO deposition, 25% of the total daytime source may arise from HONO deposited to the surface at night.

[53] In conclusion, if a HONO reservoir is formed by HONO deposition to the ground at night and is capable of being re-emitted to the atmosphere as HONO the following day, then surface emissions from this reservoir easily account for the unknown daytime HONO for nearly all cases at this location. While it is expected that the values of the individual terms governing HONO production and loss will change from location to location, expanding on our understanding of the underlying properties governing these exchange parameters, and making more measurements of these values in a variety of environments, will greatly aid in improving the ability of models to predict the production and loss of HONO in the nocturnal boundary layer, during the day, and the subsequent impact of the OH radicals released to the atmosphere by photolysis.

4. Conclusions and Atmospheric Implications

[54] The NI-PT-CIMS deployed during NACHTT-11 made 0.1 Hz HONO measurements, with automated background/interference/calibration collection, achieving detection limits of 3.8 pptv and 17% accuracy.

[55] High resolution vertical profiles of HONO revealed (i) the ground as the dominant nighttime surface on which HONO is formed from the heterogeneous reaction NO$_2$, (ii) significant amounts of HONO deposit to the ground surface at night, and (iii) the unknown daytime source of HONO is comparable to the amount of HONO that deposits to the surface at night. Total column observations of HONO and NO$_2$ allowed direct evaluation of the ground uptake coefficients for these species at night (γ$_{NO2, ground} = 2 \times 10^{-6}$ to 1.6×10^{-5} and γ$_{HONO, ground} = 2 \times 10^{-5}$ to 2×10^{-4}). Both parameters are within the ranges of laboratory and model coefficients, although it is possible that the HONO uptake coefficients observed experienced limitation by transport to the surface and may be underestimated.

[56] Daytime vertical concentration gradients indicated that the ground surface as the location of the unknown HONO source with a magnitude of 165–600 pptv h^{-1} required to account for observed mixing ratios based on known sources and sinks. The magnitude of the winter daytime HONO source at the BAO tower in February and March of 2011 was found to be consistent with the magnitude of the daytime HONO

source observations made at different locations and environments [*Elshorbany et al.*, 2009, 2012; *Kleffmann*, 2007; *Kleffmann et al.*, 2005; *Sörgel et al.*, 2011b; *Su et al.*, 2008a; *Wong et al.*, 2012; *Zhou et al.*, 2011]. A chemical model utilizing observational constraints on the HONO chemical system demonstrated that the daytime source may be dependent on a broader set of environmental variables than previously proposed and that a combination of several significant mechanisms is the most probable resolution to understanding this source. The quantity of surface-deposited HONO determined with the chemical model showed that under reasonable constraints, the integrated amount of HONO deposited to the surface at night was at least 25%, and more likely well in excess of 100%, of the integrated unknown daytime HONO source. Overall, these results suggest that if nocturnally deposited HONO forms a conserved reservoir which can be released the following day, then a significant fraction of the daytime HONO source at the BAO tower can be explained for the NACHTT-11 observation period. However, the relative magnitude of the deposition process is expected to be variable based on: (i) location, since ground surfaces are highly variable in composition, changing the uptake of HONO; and (ii) time of year, since temperature, relative humidity, other meteorological parameters, and chemical composition of the atmosphere will all have seasonal variations. Expansion of future field measurements to more explicitly address the potential for bidirectional flux of HONO from soil pore water nitrite, the fate of surface-deposited HONO, and the production of nitrite at the surface will significantly improve the ability of models to capture this chemistry. Furthermore, the reactive uptake of HONO and its pH-dependent partitioning into solutions should be explored in future laboratory investigations.

References

Acker, K., D. Möller, W. Wieprecht, F. X. Meixner, B. Bohn, S. Gilge, C. Plass-Dülmer, and H. Berresheim (2006), Strong daytime production of OH from HNO$_2$ at a rural mountain site, *Geophys. Res. Lett.*, *33*, L02809, doi:10.1029/2005GL024643.

Aldener, M., et al. (2006), Reactivity and loss mechanisms of NO$_3$ and N$_2$O$_5$ in a marine environment: Results from in situ measurements during NEAQS 2002, *J. Geophys. Res.*, *111*, D23S73, doi:10.1029/2006JD007252.

Alicke, B., A. Geyer, A. Hofzumahaus, F. Holland, S. Konrad, H. W. Pätz, J. Schäfer, J. Stutz, A. Volz-Thomas, and U. Platt (2003), OH formation by HONO photolysis during the BERLIOZ experiment, *J. Geophys. Res.*, *108*(D4), 8247, doi:10.1029/2001JD000579.

Amedro, D., A. E. Parker, C. Schoemaecker, and C. Fittschen (2011), Direct observation of OH radicals after 565 nm multi-photon excitation of NO$_2$ in the presence of H$_2$O, *Chem. Phys. Lett.*, *513*, 12–16.

Ammann, M., M. Kalberer, D. T. Jost, L. Tobler, E. Rössler, D. Piguet, H. W. Gäggeler, and U. Baltensperger (1998), Heterogeneous production of nitrous acid on soot in polluted air masses, *Nature*, *395*, 157–160.

Amoroso, A., H. J. Beine, G. Esposito, C. Perrino, M. Catrambone, and I. Allegrini (2008), Seasonal differences in atmospheric nitrous acid near Mediterranean urban areas, *Water Air Soil Pollut.*, *188*, 81–92.

Aubin, D. G., and J. P. D. Abbatt (2007), Interaction of NO$_2$ with hydrocarbon soot: Focus on HONO yield, surface modification and mechanism, *J. Phys. Chem. A*, *111*, 6263–6273.

Bartels-Rausch, T., M. Brigante, Y. F. Elshorbany, M. Ammann, B. D'Anna, C. George, K. Stemmler, M. Ndour, and J. Kleffmann (2010), Humic acid in ice: Photo-enhanced conversion of nitrogen dioxide into nitrous acid, *Atmos. Environ.*, *44*, 5443–5450.

Becker, K. H., J. Kleffmann, R. M. Negri, and P. Wiesen (1998), Solubility of nitrous acid (HONO) in ammonium sulfate solutions, *Faraday Discuss.*, *94*(11), 1583–1586.

Bedjanian, Y., and A. El Zein (2012), Interaction of NO$_2$ with TiO$_2$ surface under UV irradiation: Products study, *J. Phys. Chem. A*, *116*, 3665–3672.

Bejan, I., Y. Abd El Aal, I. Barnes, T. Benter, B. Bohn, P. Wiesen, and J. Kleffmann (2006), The photolysis of *ortho*-nitrophenols: A new gas phase source of HONO, *Phys. Chem. Chem. Phys.*, *8*, 2028–2035.

Brigante, M., D. Cazoir, B. D'Anna, C. George, and D. J. Donaldson (2008), Photoenhanced uptake of NO$_2$ by pyrene solid films, *J. Phys. Chem. A*, *112*, 9503–9508.

Bröske, R., J. Kleffmann, and P. Wiesen (2003), Heterogeneous conversion of NO$_2$ on secondary organic aerosol surfaces: A possible source of nitrous acid (HONO) in the atmosphere?, *Atmos. Chem. Phys.*, *3*, 469–474.

Brown, S. S., et al. (2013), Nitrogen, aerosol composition and halogens on a tall tower (NACHTT): Overview of a wintertime air chemistry field study in the front range urban corridor of Colorado, *J. Geophys. Res. Atmos.*, *118*, 8067–8085, doi:10.1002/jgrd.50537.

Brown, S. S., W. P. Dubé, H. D. Osthoff, D. E. Wolfe, W. M. Angevine, and A. R. Ravishankara (2007), High resolution vertical distributions of NO$_3$ and N$_2$O$_5$ through the nocturnal boundary layer, *Atmos. Chem. Phys.*, *7*, 139–149.

Chang, W. L., P. V. Bhave, S. S. Brown, N. Riemer, J. Stutz, and D. Dabdub (2011), Heterogeneous atmospheric chemistry, ambient measurements, and model calculations of N$_2$O$_5$: A review, *Aerosol Sci. Technol.*, *45*, 655–685.

Conklin, A. R. (2005), *Introduction to Soil Chemistry: Analysis and Instrumentation*, John Wiley & Sons, Inc, Hoboken, NJ.

Czader, B. H., B. Rappenglück, P. Percell, D. W. Byun, F. Ngan, and S. Kim (2012), Modeling nitrous acid and its impact on ozone and hydroxyl radical during the Texas Air Quality Study 2006, *Atmos. Chem. Phys. Discuss.*, *15*, 5851–5880.

Eisele, F. L., and D. J. Tanner (1991), Ion-assisted tropospheric OH measurements, *J. Geophys. Res.*, *96*(D5), 9295–9308.

Elshorbany, Y. F., R. Kurtenbach, P. Wiesen, E. Lissi, M. A. Rubio, G. Villena, E. Gramsch, A. R. Rickard, M. J. Pilling, and J. Kleffmann (2009), Oxidation capacity of the city air of Santiago, Chile, *Atmos. Chem. Phys.*, *9*, 2257–2273.

Elshorbany, Y. F., et al. (2012), HOx budgets during HOxComp: A case study of HOx chemistry under NOx-limited conditions, *J. Geophys. Res.*, *117*, D03307, doi:10.1029/2011JD017008.

Ensberg, J. J., M. Carreras-Sospedra, and D. Dabdub (2010), Impacts of electronically photo-excited NO$_2$ on air pollution in the South Coast Air Basin of California, *Atmos. Chem. Phys.*, *10*, 1171–1181.

Finlayson-Pitts, B. J. (2009), Reactions at surfaces in the atmosphere: Integration of experiments and theory as necessary (but not necessarily sufficient) for predicting the physical chemistry of aerosols, *Phys. Chem. Chem. Phys.*, *11*(36), 7760–7779.

Finlayson-Pitts, B. J., L. M. Wingen, A. L. Sumner, D. Syomin, and K. A. Ramazan (2003), The heterogeneous hydrolysis of NO$_2$ in laboratory systems and in outdoor and indoor atmospheres: An integrated mechanism, *Phys. Chem. Chem. Phys.*, *5*, 223–242.

Fuchs, N. A., and A. G. Stugnin (1970), *Highly Dispersed Aerosols*, Ann Arbor Science, Ann Arbor, MI.

George, C., R. Strekowski, J. Kleffmann, K. Stemmler, and M. Ammann (2005), Photoenhanced uptake of gaseous NO$_2$ on solid organic compounds: A photochemical source of HONO?, *Faraday Discuss.*, *130*, 195–210.

Gerecke, A., A. Thielmann, L. Gutzwiller, and M. J. Rossi (1998), The chemical kinetics of HONO formation resulting from heterogeneous interaction of NO$_2$ with flame soot, *Geophys. Res. Lett.*, *25*(13), 2453–2456.

Geyer, A., and J. Stutz (2004), Vertical profiles of NO$_3$, N$_2$O$_5$, O$_3$, and NO$_x$ in the nocturnal boundary layer: 2. Model studies on the altitude dependence of composition and chemistry, *J. Geophys. Res.*, *109*, D12307, doi:10.1029/2003JD004211.

Gutzwiller, L., F. Arens, U. Baltensperger, H. W. Gäggeler, and M. Ammann (2002), Significance of semivolatile diesel exhaust organics for secondary HONO formation, *Environ. Sci. Technol.*, *36*, 677–682.

Harrison, R. M., and A.-M. N. Kitto (1994), Evidence for a surface source of atmospheric nitrous acid, *Atmos. Environ.*, *28*(6), 1089–1094.

Harrison, R. M., J. D. Peak, and G. M. Collins (1996), Tropospheric cycle of nitrous acid, *J. Geophys. Res.*, *101*(D9), 14,429–14,439.

He, Y., X. Zhou, J. Hou, H. Gao, and S. Bertman (2006), Importance of dew in controlling the air-surface exchange of HONO in rural forested environments, *Geophys. Res. Lett.*, *33*, L02813, doi:10.1029/2005GL024348.

Heland, J., J. Kleffmann, R. Kurtenbach, and P. Wiesen (2001), A new instrument to measure gaseous nitrous acid (HONO) in the atmosphere, *Environ. Sci. Technol.*, *35*, 3207–3212.

Hirokawa, J., T. Kato, and F. Mafune (2008), Uptake of gas-phase nitrous acid by pH-controlled aqueous solution studied by a wetted wall flow tube, *J. Phys. Chem. A*, *112*, 12,143–12,150.

Huff, A. K., and J. P. D. Abbatt (2002), Kinetics and product yields in the heterogeneous reactions of HOBr with ice surfaces containing NaBr and NaCl, *J. Phys. Chem. A*, *106*, 5279–5287.

Kaimal, J. C., and J. E. Gaynor (1983), The Boulder Atmospheric Observatory, *J. Appl. Meteorol.*, *22*, 863–880.

Keene, W. C., J. M. Lobert, P. J. Crutzen, J. R. Maben, D. H. Scharffe, T. Landmann, C. Hély, and C. Brain (2006), Emissions of major gaseous and particulate species during experimental burns of southern African biomass, *J. Geophys. Res.*, *111*, D04301, doi:10.1029/2005JD006319.

Khalizov, A. F., M. Cruz-Quinones, and R. Zhang (2010), Heterogeneous reaction of NO₂ on fresh and coated soot surfaces, *J. Phys. Chem. A*, *114*, 7516–7524.

Kleffmann, J. (2007), Daytime sources of nitrous acid (HONO) in the atmospheric boundary layer, *Chem. Phys. Chem.*, *8*, 1137–1144.

Kleffmann, J., and P. Wiesen (2008), Technical note: Quantification of interference of wet chemical HONO LOPAP measurements under simulated polar conditions, *Atmos. Chem. Phys.*, *8*, 6813–6822.

Kleffmann, J., K. H. Becker, and P. Wiesen (1998), Heterogeneous NO₂ conversion processes on acid surfaces: Possible atmospheric implications, *Atmos. Environ.*, *32*(16), 2721–2729.

Kleffmann, J., R. Kurtenbach, J. Lörzer, P. Wiesen, N. Kalthoff, B. Vogel, and H. Vogel (2003), Measured and simulated vertical profiles of nitrous acid. Part I: Field measurements, *Atmos. Environ.*, *37*, 2949–2955.

Kleffmann, J., T. Gavriloaiei, A. Hofzumahaus, F. Holland, R. Koppmann, L. Rupp, E. Schlosser, M. Siese, and A. Wahner (2005), Daytime formation of nitrous acid: A major source of OH radicals in a forest, *Geophys. Res. Lett.*, *32*, L05818, doi:10.1029/2005GL022524.

Kleffmann, J., J. Lörzer, P. Wiesen, C. Kern, S. Trick, R. Volkamer, M. Rodenas, and K. Wirtz (2006), Intercomparison of the DOAS and LOPAP techniques for the detection of nitrous acid (HONO), *Atmos. Environ.*, *40*, 3640–3652.

Kurtenbach, R., K. H. Becker, J. A. G. Gomes, J. Kleffmann, J. Lörzer, M. Spittler, P. Wiesen, R. Ackermann, A. Geyer, and U. Platt (2001), Investigations of emission and heterogeneous formation of HONO in a road traffic tunnel, *Atmos. Environ.*, *35*, 3385–3394.

Lammel, G., and J. N. Cape (1996), Nitrous acid and nitrite in the atmosphere, *Chem. Soc. Rev.*, *25*(5), 361–369.

Lammel, G., and D. Perner (1988), The atmospheric aerosol as a source of nitrous acid in the polluted atmosphere, *J. Aerosol Sci.*, *19*(7), 1199–1202.

Langridge, J. M., R. J. Gustafsson, P. T. Griffiths, R. A. Cox, R. M. Lambert, and R. L. Jones (2009), Solar driven nitrous acid formation on building material surfaces containing titanium dioxide: A concern for air quality in urban areas?, *Atmos. Environ.*, *43*, 5128–5131.

Li, S., J. Matthews, and A. Sinha (2008), Atmospheric hydroxyl radical production from electronically excited NO₂ and H₂O, *Science*, *319*, 1657–1660.

Li, G., W. Lei, M. Zvala, R. Volkamer, S. Dusanter, P. S. Stevens, and L. T. Molina (2010), Impacts of HONO sources on the photochemistry in Mexico City during the MCMA-2006/MILAGO campaign, *Atmos. Chem. Phys.*, *10*, 6551–6567.

Li, Y., J. An, M. Min, W. Zhang, F. Wang, and P. Xie (2011), Impacts of HONO sources on the air quality in Beijing, Tianjin and Hebei Province of China, *Atmos. Environ.*, *45*, 4735–4744.

Li, X., et al. (2012), Exploring the atmospheric chemistry of nitrous acid (HONO) at a rural site in Southern China, *Atmos. Chem. Phys.*, *12*, 1497–1513.

Longfellow, C. A., T. Imamura, A. R. Ravishankara, and D. R. Hanson (1998), HONO solubility and heterogeneous reactivity on sulphuric acid surfaces, *J. Phys. Chem. A*, *102*, 3323–3332.

Miller, Y., B. J. Finlayson-Pitts, and R. B. Gerber (2009), Ionization of N₂O₄ in contact with water: Mechanism, time scales and atmospheric implications, *J. Am. Chem. Soc.*, *131*, 12,180–12,185.

Monge, M. E., B. D'Anna, L. Mazri, A. Giroir-Fendler, M. Ammann, D. J. Donaldson, and C. George (2010), Light changes the atmospheric reactivity of soot, *Proc. Natl. Acad. Sci. U. S. A.*, *107*(15), 6605–6609.

Ndour, M., B. D'Anna, C. George, O. Ka, Y. J. Balkanski, J. Kleffmann, K. Stemmler, and M. Ammann (2008), Photoenhanced uptake of NO₂ on mineral dust: Laboratory experiments and model simulations, *Geophys. Res. Lett.*, *35*, L05812, doi:10.1029/2007GL032006.

Ndour, M., P. Conchon, B. D'Anna, O. Ka, and C. George (2009), Photochemistry of mineral dust surface as a potential atmospheric

renoxification process, *Geophys. Res. Lett.*, *36*, L05816, doi:10.1029/2008GL036662.

Perner, D., and U. Platt (1979), Detection of nitrous acid in the atmosphere by differential optical absorption, *Geophys. Res. Lett.*, *6*(12), 917–920.

Petäjä, T., R. L. Mauldin III, E. Kosciuch, J. A. McGrath, T. Nieminen, P. Paasonen, M. Boy, A. Adamov, T. Kotiaho, and M. Kulmala (2009), Sulfuric acid and OH concentrations in a boreal forest site, *Atmos. Chem. Phys.*, *9*, 7435–7448.

Platt, U., D. Perner, G. W. Harris, A. M. Winer, and J. N. Pitts Jr. (1980), Observations of nitrous acid in an urban atmosphere by differential optical absorption, *Nature*, *285*, 312–314.

Qin, M., P. Xie, H. Su, J. Gu, F. Peng, S. Li, L. Zeng, J. Liu, W. Liu, and Y. Zhang (2009), An observational study of the HONO-NO₂ coupling at an urban site in Guangzhou City, South China, *Atmos. Environ.*, *43*, 5731–5742.

Ramazan, K. A., L. M. Wingen, Y. Miller, G. M. Chaban, R. B. Gerber, S. S. Xantheas, and B. J. Finlayson-Pitts (2006), New experimental and theoretical approach to the heterogeneous hydrolysis of NO₂: Key role of molecular nitric acid and its complexes, *J. Phys. Chem. A*, *110*, 6886–6897.

Reisinger, A. R. (2000), Observations of HNO₂ in the polluted winter atmosphere: Possible heterogeneous production on aerosols, *Atmos. Environ.*, *34*(23), 3865–3874.

Riedel, T. P., et al. (2012), Nitryl chloride and molecular chlorine in the coastal marine boundary layer, *Environ. Sci. Technol.*, *46*, 10,463-70, doi:10.1021/es204632r.

Roberts, J. M., et al. (2010), Measurement of HONO, HNCO, and other inorganic acids by negative-ion proton-transfer chemical-ionization mass spectrometry (NI-PT-CIMS): Application to biomass burning emissions, *Atmos. Meas. Tech.*, *3*, 981–990.

Sörgel, M., I. Trebs, A. Serafimovich, A. Moravek, A. Held, and C. Zetzsch (2011a), Simultaneous HONO measurements in and above a forest canopy: Influence of turbulent exchange on mixing ratio differences, *Atmos. Chem. Phys.*, *11*, 841–855.

Sörgel, M., et al. (2011b), Quantification of the unknown HONO daytime source and its relation to NO₂, *Atmos. Chem. Phys.*, *11*(20), 10,433–10,447.

Spicer, C. W., R. W. Coutant, G. F. Ward, D. W. Joseph, A. J. Gaynor, and I. H. Billick (1989), Rates and mechanisms of NO₂ removal from indoor air by residential materials, *Environ. Int.*, *15*, 643–654.

Stemmler, K., M. Ammann, C. Donders, J. Kleffmann, and C. George (2006), Photosensitized reduction of nitrogen dioxide on humic acid as a source of nitrous acid, *Nature*, *440*, 195–198.

Stemmler, K., M. Ndour, Y. F. Elshorbany, J. Kleffmann, B. D'Anna, C. George, B. Bohn, and M. Ammann (2007), Light induced conversion of nitrogen dioxide into nitrous acid on submicron humic acid aerosol, *Atmos. Chem. Phys.*, *7*, 4237–4248.

Stutz, J., B. Alicke, and A. Neftel (2002), Nitrous acid formation in the urban atmosphere: Gradient measurements of NO₂ and HONO over grass in Milan, Italy, *J. Geophys. Res.*, *107*(D22), 8192, doi:10.1029/2001JD000390.

Stutz, J., B. Alicke, R. Ackermann, A. Geyer, S. Wang, A. B. White, E. J. Williams, C. W. Spicer, and J. D. Fast (2004), Relative humidity dependence of HONO chemistry in urban areas, *J. Geophys. Res.*, *109*, D03307, doi:10.1029/2003JD004135.

Stutz, J., H.-J. Oh, S. I. Whitlow, C. Anderson, J. E. Dibb, J. H. Flynn, B. Rappenglück, and B. Lefer (2010), Simultaneous DOAS and mist-chamber IC measurements of HONO in Houston, TX, *Atmos. Environ.*, *2010*(44), 4090–4098.

Su, H., Y. F. Cheng, M. Shao, D. F. Gao, Z. Y. Yu, L. M. Zeng, J. Slanina, Y. H. Zhang, and A. Wiedensohler (2008a), Nitrous acid (HONO) and its daytime sources at a rural site during the 2004 PRIDE-PRD experiment in China, *J. Geophys. Res.*, *113*, D14312, doi:10.1029/2007JD009060.

Su, H., Y. F. Cheng, P. Cheng, Y. H. Zhang, S. Dong, L. M. Zeng, X. Wang, J. Slanina, M. Shao, and A. Wiedensohler (2008b), Observation of nighttime nitrous acid (HONO) formation at a non-urban site during PRIDE-PRD2004 in China, *Atmos. Environ.*, *42*, 6219–6232.

Su, H., Y. Cheng, R. Oswald, T. Behrendt, I. Trebs, F. X. Meixner, M. O. Andreae, P. Cheng, Y. Zhang, and U. Pöschl (2011), Soil nitrite as a source of atmospheric HONO and OH radicals, *Science*, *333*, 1616–1618.

Tanner, D. J., A. Jefferson, and F. L. Eisele (1997), Selected ion chemical ionization mass spectrometric measurement of OH, *J. Geophys. Res.*, *102*(D5), 6415–6425.

Veres, P., J. M. Roberts, C. Warneke, D. Welsh-Bon, M. S. Zahniser, S. C. Herndon, R. Fall, and J. A. de Gouw (2008), Development of negative-ion proton-transfer chemical-ionisation mass spectrometry (NI-PT-CIMS) for the measurement of gas-phase organic acids in the atmosphere, *Int. J. Mass Spectrom.*, *274*, 48–55.

Veres, P., et al. (2011), Evidence of rapid production of organic acids in an urban air mass, *Geophys. Res. Lett.*, *38*, L17807, doi:10.1029/2011GL048420.

Villena, G., J. Kleffmann, R. Kurtenbach, P. Wiesen, E. Lissi, M. A. Rubio, G. Croxatto, and B. Rappenglück (2011), Vertical gradients of HONO, NO_x and O_3 in Santiago de Chile, *Atmos. Environ.*, *45*, 3867–3873.

Vogel, B., H. Vogel, J. Kleffmann, and R. Kurtenbach (2003), Measured and simulated vertical profiles of nitrous acid. Part II. Model simulations and indications for a photolytic source, *Atmos. Environ.*, *37*, 2957–2966.

Volkamer, R., P. Sheehy, L. T. Molina, and M. J. Molina (2010), Oxidative capacity of the Mexico City atmosphere. Part 1: A radical source perspective, *Atmos. Chem. Phys.*, *10*, 6969–6991.

Wagner, N. L., W. P. Dubé, R. A. Washenfelder, C. J. Young, I. B. Pollack, T. B. Ryerson, and S. S. Brown (2011), Diode laser-based cavity ring-down instrument for NO_3, N_2O_5, NO, NO_2 and O_3 from aircraft, *Atmos. Meas. Technol.*, *4*, 1227–1240.

Wojtal, P., J. D. Halla, and R. McLaren (2011), Pseudo steady states of HONO measured in the nocturnal marine boundary layer: A conceptual model for HONO formation on aqueous surfaces, *Atmos. Chem. Phys.*, *11*, 3243–3261.

Wong, K. W., and J. Stutz (2010), Influence of nocturnal vertical stability on daytime chemistry: A one-dimensional model study, *Atmos. Environ.*, *44*, 3753–3760.

Wong, K. W., H.-J. Oh, B. Lefer, B. Rappenglück, and J. Stutz (2011), Vertical profiles of nitrous acid in the nocturnal urban atmosphere of Houston, TX, *Atmos. Chem. Phys.*, *11*, 3595–3609.

Wong, K. W., C. Tsai, B. Lefer, C. Haman, N. Grossberg, W. H. Brune, X. Ren, W. Luke, and J. Stutz (2012), Daytime HONO vertical gradients during SHARP 2009 in Houston, TX, *Atmos. Chem. Phys.*, *12*, 635–652.

Young, C. J., et al. (2012), Vertically resolved measurements of nighttime radical reservoirs in Los Angeles and their contribution to the urban radical budget, *Environ. Sci. Technol.*, *46*, 10,965–10,973.

Young, A. H., W. C. Keene, A. A. P. Pszenny, R. Sander, J. A. Thornton, T. P. Riedel, and J. R. Maben (2013), Phase partitioning of soluble trace gases with size-resolved aerosols in near-surface continental air over northern Colorado, USA during winter, *J. Geophys. Res. Atmos.*, doi:10.1002/jgrd.50655.

Yu, Y., B. Galle, A. Panday, E. Hodson, R. Prinn, and S. Wang (2009), Observations of high rates of NO_2-HONO conversion in the nocturnal atmospheric boundary layer in Kathmandu, Nepal, *Atmos. Chem. Phys.*, *9*, 6401–6415.

Zhang, N., X. Zhou, P. B. Shepson, H. Gao, M. Alaghmand, and B. Stirm (2009), Aircraft measurement of HONO vertical profiles over a forested region, *Geophys. Res. Lett.*, *36*, L15820, doi:10.1029/2009GL038999.

Zhou, X., H. Gao, Y. He, G. Huang, S. Bertman, K. Civerolo, and J. J. Schwab (2003), Nitric acid photolysis on surfaces in low-NO_x environments: Significant atmospheric implications, *Geophys. Res. Lett.*, *30*(23), 2217, doi:10.1029/2003GL018620.

Zhou, X., et al. (2011), Nitric acid photolysis on forest canopy surface as a source for tropospheric nitrous acid, *Nat. Geosci.*, *4*, 440–443.

Ziemba, L. D., J. E. Dibb, R. J. Griffin, C. Anderson, S. I. Whitlow, B. Lefer, B. Rappenglück, and J. H. Flynn (2010), Heterogeneous conversion of nitric acid to nitrous acid on the surface of primary organic aerosol in an urban atmosphere, *Atmos. Environ.*, *44*, 4081–4089.